Simultaneous ex-situ CO_2 mineral sequestration and hydrogen production from olivine-bearing mine tailings

[a,b] *Kanchana Kularatne

*corresponding author

[a]IFP Energies Nouvelles, 1- 4 Avenue du Bois Préau, 92852 Rueil-Malmaison, France

[b]Institut de Physique du Globe de Paris, Sorbonne Paris Cité, Université Paris Diderot, UMR 7154 CNRS, 1 rue Jussieu, F-75005 Paris, France

e mail : kularatne@ipgp.fr

Present address: Institut de Physique du Globe de Paris, 1 rue Jussieu, F-75005 Paris, France

[a]Olivier Sissmann

[a]IFP Energies Nouvelles, 1- 4 Avenue du Bois Préau, 92852 Rueil-Malmaison, France

e mail : olivier.sissmann@ifpen.fr

[a]Eric Kohler

[a]IFP Energies Nouvelles, 1- 4 Avenue du Bois Préau, 92852 Rueil-Malmaison, France

e mail : eric.kohler@ifpen.fr

[a]Michel Chardin

[a]IFP Energies Nouvelles, 1- 4 Avenue du Bois Préau, 92852 Rueil-Malmaison, France

e mail : michel.chardin@ifp.fr

[a]Sonia Noirez

[a]IFP Energies Nouvelles, 1- 4 Avenue du Bois Préau, 92852 Rueil-Malmaison, France

e mail : sonia.noirez@ifp.fr

[b]Isabelle Martinez

[b]Institut de Physique du Globe de Paris, Sorbonne Paris Cité, Université Paris Diderot, UMR 7154 CNRS, 1 rue Jussieu, F-75005 Paris, France

e mail : martinez@ipgp.fr

Abstract

Hydrothermal alteration batch experiments were conducted on olivine bearing mine tailings in order to investigate two potential valorization methods: the ex-situ CO_2 sequestration and hydrogen production. The originality of this work lies in the simultaneous investigation of these two processes. We reacted powdered mine tailings with CO_2-saturated water at three different sets of P/T conditions, 473K/ 15 MPa, 523 K/30 MPa and 573K/30 MPa. After 25 days of reaction, CO_2 was sequestered in the form of Fe-bearing magnesite, $(Mg,Fe)CO_3$ in all the experiments. Maximum carbonation yield was achieved at 523 K and 30 MPa, which was 53.8 wt.% of product, equivalent to the trapping of 320.5 g of CO_2 per kg of mine tailings. Hydrogen gas was produced via the oxidation of Fe^{2+} in olivine. The highest quantity of hydrogen (H_2) was produced at 573 K/ 30 MPa which was 0.57 g of H_2 per kg of mine tailings. It suggests that the temperatures between 523 K and 540 K at pCO_2=30 MPa are favorable for simultaneous ex-situ CO_2 mineral sequestration and hydrogen production from New Caledonian mine tailings.

The combined method of ex-situ CO_2 storage and hydrogen production proposed by this study offsets 90% of New Caledonia's annual CO_2 emissions while compensating ~10 % of New Caledonia's annual energy demand. More globally, it has implications for cost effective disposal of industrial CO_2 emissions and production of hydrogen gas (clean energy) at a large scale; those two processes could be combined using the residual heat provided by a third one such as the high temperature smelting of ore.

Key words: New Caledonia, Nickel, Carbonation, Hydrogen, Hydrothermal, Olivine, Glass

1. Introduction

Since the industrial revolution, the atmospheric carbon dioxide (CO_2) level has been substantially increased up to its present day value of ~407 ppm (NOAA, 2016), eventually causing enormous climatic changes such as global warming, ocean acidification, and glacial melting (Manabe and Stouffer, 1993, Kondo et al., 2018; Zhang et al., 2017; Caecer et al., 2018; Marzeion et al., 2018). Up to 65% of the global CO_2 emissions were attributed to fossil fuel combustion (Edenhofer et al., 2014), directing the CO_2 mitigation measures essentially towards CO_2 sequestration mechanisms and introduction of alternate energy sources to fossil fuels.

Scientists have considered the CO_2 sequestration in minerals as the so-called permanent method to capture and store industrial emissions of CO_2. This method was first suggested by Seifritz (1990), based on the natural phenomena of silicate weathering into carbonates (Abu-Jaber and Kimberley, 1992; Ece et al., 2005; Lugli et al., 2000; Oskierski et al., 2013; Palinkaš et al., 2012; Zedef et al., 2000), during which CO_2 reacts with silicates precipitating thermodynamically stable solid carbonates as given by the generalized equation below:

$$M_xSi_yO_{(x+2y-n)}(OH)_{2n} + xCO_2 = xMCO_3 + ySiO_2 + nH_2O \quad \text{(Eq. 1)}$$

where (M^{2+}) represents a divalent cation such as, Fe^{2+}, Mg^{2+} and Ca^{2+} in a silicate mineral, and MCO_3 thus represents the carbonate incorporating the element M. Once CO_2 is converted into a carbonate following reaction (1), it will not be released into the atmosphere over geological time scales.

For the last three decades various aspects of CO_2 mineral sequestration have been experimentally investigated, on several mafic minerals such as olivine, serpentine, and pyroxenes (Johnson et al., 2014; Béarat et al., 2006; King et al., 2010; Sissmann et al., 2013; Daval et al., 2009a; Wolff-Boenisch et al., 2006., Park et al., 2003). Among the minerals which consist of divalent Ca, Mg or Fe in their structure, olivine ($(Mg,Fe)_2SiO_4$) is considered the most

favorable for carbonation due to several reasons. Firstly, olivine is abundant in nature in mafic and ultramafic environments (e.g. basalt, peridotites, and dunites). Secondly, it's one of the fastest dissolving silicates (Guthrie, 2001; Brantley, 2003; Golubev et al., 2005; Wolff-Boenisch et al., 2006). Olivine, which contains both Fe and Mg, may form Fe-bearing magnesite ($(Mg,Fe)CO_3$) during the carbonation process, according to equation (2):

$$(Mg,Fe)_2SiO_{4(s)} + 2CO_{2(aq)} \rightarrow 2(Mg,Fe)CO_{3(s)} + SiO_{2(aq)} \quad \text{(Eq. 2)}$$

Gerdemann et al. (2007), who conducted carbonation experiments on olivine under a wide range of temperature (298 K < T < 523 K) and CO_2 partial pressure (1 MPa< pCO_2 < 25 MPa), have shown that olivine (<75 μm) could be carbonated efficiently, with ca. 85% completion of reaction within an extremely short period of time (around 6 hours), by reacting with a solution of 0.64M $NaHCO_3$ + 1M NaCl, at T = 458 K and pCO_2 = 15 MPa. This study also demonstrated that the extent of olivine carbonation is directly proportional to the CO_2 partial pressure in the system (pCO_2). In addition, the authors showed that, at a given pCO_2, the extent of carbonation was negligible at lower temperatures (<363 K), while a decrease in the extent of reaction was observed at high temperatures (>458 K). It indicated that at low temperatures, the carbonation reaction is kinetically not favorable due to slow mineral dissolution, whereas if the temperature is too high, although mineral dissolution is kinetically favorable, the extent of carbonation nevertheless decreases. This is due to the formation of Mg-rich phyllosilicates during the competing reaction of serpentinization, in which extensive oxidation of Fe^{2+} also occurs, producing hydrogen, as shown by:

$$\underset{\text{(olivine)}}{(Mg,Fe)_2SiO_4} + nH_2O \rightarrow \underset{\text{(serpentine)}}{x(Mg,Fe^{2+}, Fe^{3+})_3(Si,Fe^{3+})_2O_5(OH)_4} + \underset{\text{(brucite)}}{y(Mg,Fe)(OH)_2} + \underset{\text{(magnetite)}}{zFe_3O_4} + (n-2x-y)\,H_2 \quad \text{(Eq. 3)}$$

The stoichiometric parameters n, x, y and z in this equation strongly depend on how iron is partitioned among the reaction products (McCollom et al., 2016). Large quantities of

hydrogen are added to the deep sea floor by this reaction which takes place at the mid oceanic ridge hydrothermal systems. A number of studies reported the temperature, thermodynamic, and compositional controls on serpentinization (Janecky and Seyfried, 1986; Klein et al., 2013, 2009; Klein and Garrido, 2010; McCollom et al., 2016; McCollom and Bach, 2009a; Seyfried et al., 2007). Two important information from these studies indicate that high temperatures (~573 K) favor large quantities of hydrogen due to (i) an increase of overall reaction rate of serpentinization, and (ii) an increased partitioning of Fe into brucite ($Mg(OH)_2$), rather than into magnetite (Fe_3O_4). In addition to the hydrothermal alteration of olivine, pure iron or iron-rich materials have also been experimentally studied for hydrogen production (Crouzet et al., 2017; Malvoisin et al., 2013).

Olivine, which contains both Mg and Fe, could therefore be favorable for simultaneous CO_2 mineral sequestration and hydrogen production, when reacting within a specific range of pressure, temperature and pH conditions, under which carbonation and serpentinization reactions will not inhibit one another. Therefore, this method is a clear improvement on current CO_2 mitigation methods, as it proposes reduction of CO_2 emissions by mineral storage, and also hydrogen production which is a green energy source. Compared to Fe-Mg-bearing pure minerals or rocks, mine tailings serve as an alternative source of mineral alkalinity that are readily and cheaply available (Bobicki et al., 2012), and can be valorized by the above method (Bobicki et al., 2012; Harrison et al., 2016, 2013; Power et al., 2013; Wilson et al., 2014; Malvoisin et al, 2013). However, these previous studies on mine tailings have only focused on either CO_2 storage or H_2 production separately. The present study aims to investigate the potential of combining the strategy of CO_2 mineral storage with hydrogen production by reacting olivine-bearing mine waste material obtained from nickel (Ni) extraction mines in New Caledonia. In order to maintain both of these reactions, the mine tailings were reacted with CO_2-saturated water at P/T range slightly inferior to the conditions previously identified as optimum for ex-situ

carbonation (Gerdemann et al., 2007), and close to optimum hydrogen production in hydrothermal systems (McCollom et al., 2016; McCollom and Bach, 2009a; McCollom and Bach, 2008; Tutolo et al., 2018; Meyhew et al., 2018). We present the quantities of CO_2 that can be stored in mine tailings, and the quantities of H_2 that can be produced by this method. Based on these experimental values, we estimated the CO_2 offset and compensation of energy demand of New Caledonia. Although the application of this process is centered on New Caledonian mine tailings, it could be translated to other industrial sites where Mg and Fe remain major components of the wastes after ore processing.

2. Materials and methods

2.1 Starting materials

All the experiments were performed on olivine bearing mine tailings from industrial nickel (Ni) extraction sites in New Caledonia, where Ni is extracted from laterite and saprolite ores (Wacaster, 2013). The hand specimens of mine tailings consisted of light- to dark-green irregular shaped grains with sizes ranging from few millimeters to < 1 cm. The X-ray diffraction (XRD) analysis performed on a finely powdered sample indicated the presence of olivine, traces of enstatite and an amorphous phase (glass). The amount of glass was quantified by XRD Rietveld analysis performed on the diffraction pattern of a mixture of powdered mine tailings and alumina (20 wt.%) where alumina serves as the internal standard (Bish and Howard, 1988; Bish and Post, 1993; McCusker et al., 1999). According to this analysis the sample was composed of 55 wt.% of glass and 45 wt.% of crystalline olivine. The chemical composition of mine tailings was obtained by electron probe micro analysis (EPMA) operated at 15 keV and 40 nA, on few randomly selected macroscopic grains mounted on epoxy resin. The analysis was performed on multiple points on glass and olivine, which appeared texturally different under SEM, and the average compositions were reported in Table 1. This is in good agreement with

150 the composition reported by Bodénan et al. (2014), who used the same material for CO_2
151 sequestration experiments. The magnesium numbers (Mg#=Mg/(Mg+Fe)) of the glass and
152 crystalline olivine were 0.75 and 0.88 respectively, and were calculated on molar basis using the
153 average oxide wt.%.

154 Mine tailings were crushed in a ball mill to obtain 40 - 63 µm size fraction. This size
155 fraction was chosen in order to maintain rapid dissolution kinetics, as well as to facilitate
156 microscopic observations. Furthermore, those grain sizes are in the same range than those used
157 in the few previous studies on hydrogen generation (Malvoisin et al., 2013, 2012a, 2012b), thus
158 making the comparison easier. Even though the choice of nano-scale particles could have
159 provided a considerably faster reaction, the mineral surfaces available for microscopic studies of
160 the products would have been limited. Finally, for industrial purposes, grinding large quantities
161 of solid down to the nanometer scale would largely increase the cost of the process.

162 The selected sieve fraction was subsequently ultrasonically cleaned in ethanol for 8-
163 10 min to remove the fine particles adhered to the surface. This process was repeated until the
164 supernatant became clear. The powder was dried in oven at 343 K overnight after cleaning with
165 ultra-pure de-ionized water (electrical conductivity = 18.2 MΩ cm). Very few fine particles
166 remained adhering to the grain surfaces of the above dried powder, when observed under SEM
167 (Figure 1a). The specific surface area (SSA) of the cleaned starting powder was determined by
168 Kr adsorption analysis, according to the Brunauer–Emmett–Teller (BET) method (Brunauer et
169 al., 1938), yielding a value of 0.23 m^2/g.

170 Scanning electron microscopic (SEM) analysis performed on a polished section of
171 mine tailings indicate that it consists of inclusion of free and textured glass with embedded
172 olivine crystals, resulting in a “dendritic texture” or a “quench texture” (Figure 1b). The glass
173 and dendritic texture were assumed to be the result of two steps in the ore processing. The first
174 is the “calcination” performed by pre heating the ore at >1173 K for moisture removal and first

phase of metal oxide reduction. The second is the “fusion reduction” by which the ore is melted using an electrode operated at <1973 K, separating Ni from the residue or mine tailings. We assume that these conditions reached the “dry” melting-point of peridotite (-approximate composition for the ophiolite) under atmospheric pressure (Takahashi, 1986), where olivine can coexist with pyroxene melt up to about 2023 K at 1 atm during the eutectic melting of peridotite, which could probably explain the quench texture in mine tailings.

2.2 High pressure and high temperature experiments

Three batch experiments were conducted at different P/T conditions, in order to investigate the most favorable conditions for simultaneous CO_2 sequestration and H_2 production. All the experiments were performed in 250 ml volume Parr® hastelloy stirring- type batch reactors (impeller speed, 100 r.p.m), with a TiO_2 inner lining. Powdered mine tailings and deionized water (1:100 mass ratio) were added to the batch reactors and pressurized with CO_2 (99.9% purity).

The first experiment (MT1) was conducted at 473K/ 15 MPa, which was slightly above the known optimum temperature reported for the CO_2 mineral sequestration, i.e. 453 K/15 MPa, using a solution of 0.64M $NaHCO_3$/1M NaCl. The second and third experiments were conducted at P/T conditions more favorable for H_2 production by serpentinization, such as 473 K and 673 K and 30-50 MPa (Allen and Seyfried, 2003; Andreani et al., 2012; Berndt et al., 1996; Janecky and Seyfried, 1986; Malvoisin et al., 2012a; McCollom and Bach, 2009b; McCollom and Seewald, 2001). These conditions are known to accelerate the serpentinization rate while producing large amounts of H_2. The second experiment (MT2) was thus conducted at 523 K/30 MPa, both temperature and pressure being slightly above MT1. The third experiment (MT4) was performed at 573 K/30 MPa. Two more experiments were conducted as blank runs (MT2b, and MT4b) to determine possible contaminations in gas phase. They were conducted under similar conditions (-in terms of amount of water, pCO_2, T) to those of MT2 and MT4, but

without any solid phases added in the reactor. Details of these experiments are reported in Table 2. The run duration of all the experiments was approximately 25 days. The pCO_2 of the experiments drops intermittently (0.1 to 0.5 MPa) during the run due to; (i) CO_2 consumption by carbonation reaction, and (ii) sampling out aliquots of gas from the batch reactor. The pressure was re-adjusted to the initial pressure by pumping CO_2 gas back to the batch reactor. At the end of the 25-days run, the experiments were quenched rapidly to ambient conditions by cooling the reactor cell in a water bath for ~20-30 min. The autoclaves were then opened right after releasing the pressurized CO_2 inside the reactor, minimizing the potential formation of secondary products at this stage. The solid products were recovered and oven-dried at 333 K overnight, then used for further analysis, as described below.

At these P/T conditions, most of the CO_2 pumped into the reactor exists as $CO_{2(aq)}$ with a smaller amount of $HCO_3^-{}_{(aq)}$ and traces of $CO_3^{-2}{}_{(aq)}$, which can therefore be summed up to a binary mixture of CO_2-H_2O that has not reached critical condition. The initial pH at P/T relevant to experimental conditions was calculated by the CHESS geochemical code (van der Lee and De Windt, 2002) for each reaction temperature, creating a closed system with water and CO_2 (fCO_2 at each P/T conditions was calculated using the Thermosolver program (Barnes and Koretsky, 2004). The experimental conditions and the calculated initial pH of the solutions are reported in Table 2.

2.3 Sampling and analytical methods

2.3.1 Gas sampling and analysis

The gas phase in the head space of the batch reactor was sampled every 2-3 days during the reaction, by connecting a gas-sampling tube to the batch reactor. Before sampling, a vacuum of 10^{-5} bars was created along the tubings of the batch reactor and also in the sampling tube. The vacuum was held for about 10-15 min. This procedure ensures the absence of any leak and contaminations in the tubings. Collected gas samples were then analyzed with a Varian CP-3800 gas chromatograph (GC) to identify and quantify the gaseous products of the reaction. For this purpose, two standards were first analyzed: one with an atmospheric composition, and the other being a mixture of H_2, He, N_2, CO_2 and alkanes up to four carbons (C_1-C_4). The samples and the standards were injected to the GC at ~1200 mbar at room temperature. Before analyzing a standard or a sample, a blank measurement was carried out by injecting N_2. Finally, the percentages (%) of each gas in the analyzed samples were calculated using the response factors (k) obtained. The uncertainty on H_2, CO_2, CH_4 and other simple alkanes abundances (C_2-C_4) measured by GC were 5.4%, 1.3%, 0.6% and ~1.2% respectively.

2.3.2 Solid product analysis

The mineralogical composition of bulk solid products was obtained through XRD analysis performed on finely powdered reaction products, using a X'Pert PRO (PANalytical) x-ray diffractometer with a Cu anode (Cu Kα = 1.5418 Å), operated under 45 kV and 40 mA. The detection limit of XRD is ~1%. Rock-Eval 6 analysis was performed for better detection and quantification of carbonate. The quantification limit of Rock-Eval 6 is ~0.02 wt.% C, which corresponds to ~0.15 wt.% $MgCO_3$; this method is one order of magnitude more sensitive than the phase quantification by XRD. More details on sample preparation, instrumentation and analysis of the Rock-Eval 6 technique can be found in Behar et al. (2001) and Lafargue et al.

(1998). The analytical details and the calculation of carbonates are reported in supporting information S6. Energy dispersive X-ray analysis in transmission electron microscope (TEM-EDX) was performed on ultra-thin sections prepared by focused ion beam milling (FIB), in order to obtain the composition of magnesite: more details are given in supporting information S10.

A separate fraction of the reaction products was mounted on adhesive carbon-taped sample holders, gold (Au) coated and observed under "high vacuum" conventional SEM, EVO MA 10, Carl Zeiss SMT with a tungsten filament operated under 15 kV and 100 mA. A 150 pA beam was applied for secondary electron (SE) imaging to observe the surface topography with a high spatial resolution, while the back scattered electron detector (BSE) was used to obtain images with atomic number contrast. Qualitative chemical analyses were performed by energy dispersive X-ray analysis (EDX), with a probe current at 700 to 750 pA (Oxford). The silicon drift detector is calibrated on cobalt (Co) for quantitative analyzes during 10 s at 10 to 15 kcps with a dead time of about 15 s. In addition, SEM element mapping was performed on the reaction products mounted on epoxy resin, finely polished by ion beam milling.

2.3.3 Fe(III) / Fe(II) analysis

The amounts of Fe^{2+} and total iron in the non-reacted mine tailings, and the three experimental products were analyzed at the Centre de Recherches Pétrographiques et Géochimiques (CRPG), Nancy, France. The samples were boiled in HF / H_2SO_4 to release Fe^{2+} which was then quantified by volumetric titration with $K_2Cr_2O_3$. Another fraction of the sample was then heated with $LiBO_2$ at 1223 K and acid digested (4 vol.% HNO_3) to convert all species of iron (e.g. Fe^0 and Fe^{2+}) contained in the sample into Fe_2O_3 (Fe^{3+}). The resulting ferric iron was measured by atomic absorption spectrophotometer (AAS). The amount of Fe^{3+} in the non-reacted mine tailings sample was calculated by subtracting the Fe^{2+}molar amount measured in

the FeO analysis from the (Fe^{2+} + Fe^{3+}) amount measured in the Fe_2O_3 analysis. The value being close to 0 suggests there is little to no oxidized iron in the initial material. The quantities of H_2 measured by GC at the end of the experiments were compared to the amounts calculated from the loss of Fe^{2+} (through oxidation and simultaneous H_2 production) in the products. In order to estimate the amount of Fe^{3+} formed during the experiments, the amount of Fe^{2+} measured in the products were subtracted from the one measured in the initial non-reacted mine tailings; the quantity of H_2 produced was then extrapolated from the oxidized iron (Fe^{3+}) according to:

$$2Fe^{2+}_{(aq)} + 2H_2O_{(l)} = 2Fe^{3+}_{(aq)} + 2OH^-_{(aq)} + H_{2(g)} \quad \text{(Eq. 4)}$$

where, the stoichiometric proportion of Fe^{2+} : H_2 is 2:1.

3. Results

3.1 Secondary products

XRD pattern of non-reacted mine tailings and the reaction products of three experiments are shown in Figure 2c. The non-reacted mine tailings sample primarily consisted of olivine. The peaks of corundum (Figure 2c), in this diffraction pattern are due to pure corundum which was added to mine tailings as the internal standard for quantification of glass. The products consisted of Fe-rich magnesite as the major phase, small quantities of phyllosilicates and traces of non-reacted olivine (Figure 2c). Fe-bearing magnesite was identified by the characteristic reflections at 2θ = 35.9° and 50° (Giammar et al., 2005; Garcia et al., 2010). SEM element mapping performed on a polished section of MT2 sample showed the presence of abundant magnesite compared to other phases such as olivine, glass, and phyllosilicate, and therefore is well in agreement with the XRD results (Figure 2a). The SEM analysis performed on a carbon-coated reaction product of the same sample indicates the growth of rhombohedral magnesite containing both Fe and Mg, as confirmed by the EDX spectra collected on SEM (Figure 2b). Figure 3 shows the SEM analysis performed on polished sections of solid products of the three

experiments, each mounted on epoxy resin. At 473 K /15 MPa, mine tailings have been altered, precipitating anhedral magnesite, and thin layers of phyllosilicate (Figure 3a). Magnesites precipitated along a grain of textured mine tailings are shown on Figure 3b. At 523 K /30 MPa, the product contained thick phyllosilicate layers around mine tailings and subhedral magnesite with Fe and Mg compositional zoning (Figure 3c). At 573 K /30 MPa, the products contained anhedral magnesites and mine tailings heavily covered by a thick fibrous phyllosilicate layer (Figure 3c). More SEM images with EDX analysis on these samples are given in supplementary S7, S8 and S9. The chemical composition of magnesites analyzed by TEM-EDX yielded $Mg_{0.92}Fe_{0.08}CO_3$, $Mg_{0.58}Fe_{0.42}CO_3$ and $Mg_{0.83}Fe_{0.17}CO_3$ at 473 K /15 MPa, 523 K /30 MPa and 573 K /30 MPa respectively, showing different concentrations of iron further discussed in section 4.2. The details of TEM analysis is given in supplementary information S10.

Compared to the diffraction pattern of the non-reacted sample, the peak intensity of olivine gradually decreases with the increasing temperature of the experiments, indicating olivine dissolution has mostly increased along with temperature. The semi-quantitative phase analysis on the collected diffraction patterns indicated that approximately 23.3 wt.%, 9.4 wt.% and 12.2 wt.% of olivine were still remaining in the reaction products of 473 K /15 MPa, 523 K /30 MPa and 573 K /30 MPa experiments respectively. The peaks for phyllosilicates are broad and less intense in all experiments, and the number of phyllosilicate peaks visible on the diffractogram increased with temperature, indicating more phyllosilicates formed with higher temperature. A preliminary identification of these phyllosilicates was obtained by applying a treatment with ethylene glycol to verify their expansion properties, which suggested that they were smectite clay minerals. However, due to the inherent limitations of the equipment, the amount of phyllosilicate and remaining glass could not be quantified separately.

3.2 Carbonate yield

The presence of carbonates and their precise quantification were further confirmed using the Rock-Eval 6 technique. The only carbonate phase produced in all the experiments were Fe-bearing magnesites, $(Mg,Fe)CO_3$, in accordance with the results of XRD analysis. Carbonate quantification by Rock-Eval 6 resulted in 20.3%, 44.9% and 21.6% at 473 K/ 15 MPa, 523 K/ 30 MPa and 573 K/ 30 MPa respectively (the calculation is given in S6); those carbonation yields are averages of duplicate experiments. These yields suggest that 1.00 kg of mine tailings could capture 115g, 321g and 119 g of gaseous CO_2 by a reaction with pure water at 473 K/ 15 MPa, 523 K/ 30 MPa and 573 K/ 30 MPa, respectively (Table 2 and S6).

3.3 Hydrogen production

As the starting mine tailings material is iron-rich (average of 10.9 wt.%), its reaction with water at high pressure and high temperature leads to the production of H_2, as a result of iron oxidation through water reduction (also written for the serpentinization reaction given by eq.3). However, the produced hydrogen in all the experiments is approximately three orders of magnitude lower than the CO_2 in the gas phase, since CO_2 was injected to reach a total pressure of either 15 or 30 MPa. The variations in gas phase composition in each experiment are given below.

At 473 K and 15 MPa: Figure 4a, illustrates the cumulative production of hydrogen as a function of time for MT1. Hydrogen was produced gradually reaching a maximum of 20.0 µmol/g of mine tailings after 25 days of reaction, which indicates that the reaction is still in progress. The maximum hydrogen production of 20.0 µmol/g is equivalent to producing around 0.04 g of H_2 for 1.0 kg of mine tailings. Hydrogen was produced at a rate of approximately 0.7 µmol/g/day, obtained by the gradient fitted though the data. Traces of methane (<0.30 µmol/g)

were detected in the gas phase after 9.8 days of reaction, but other light hydrocarbons (C_2-C_4) were not detected (S 1).

At 523 K and 30 MPa: The cumulative hydrogen production as a function of reaction time of MT2 experiment is shown in Figure 4b. Hydrogen continues to be produced at a rate of 1 µmol/g/day until ~9 days, as the reaction proceeds. After 9 days, hydrogen production increases abruptly and then continues to increase at a rate of 3.2 µmol/g/day. The maximum amount of gaseous hydrogen measured in this experiment was 117.6 µmol/g or 0.24 g/kg of mine tailings, which is approximately 5 times more than in MT1. No hydrogen was detected in the gas phase of an experimental blank (MT2b) conducted under the same without adding mine tailings confirming that hydrogen was produced only by reaction between pure water and mine tailings (Figure 4b). Light hydrocarbons such as CH_4, C_2H_6, C_3H_8 and C_4H_{10} were also observed in the gas phases of both the experiment and experimental blank, but in trace quantities (S2 and S4).

At 573 K and 30 MPa: Cumulative hydrogen production of MT4 experiment is shown in Figure 4c. At the initial stage, hydrogen was produced at a rate of 21 µmol/g/day ($0<t<8.8$ days), reaching a maximum of 283.5 µmol/g or 0.57 g/kg. This is the highest quantity of hydrogen produced among all three experiments, and is confirmed by the H_2 production inferred from iron (III) measured at the end of the experiments (265 µmol/g, see Table 2). Then, the amount of hydrogen decreased drastically, reaching a plateau with an average of 41 µmol/g (Figure 4c). Similarly to MT2, hydrogen was not detected in the gas phase of an experimental blank (MT4b) conducted at the same P/T conditions, which confirmed there was no contamination of hydrogen in the experiment (Figure 4c and S3). This decrease in cumulative hydrogen could be explained by the formation of short-chained organic molecules through its interaction with CO_2, as discussed by Seewald (2006). In addition, CH_4, C_2H_6, C_3H_8 and C_4H_{10} were detected in the gas phase, in which the detected methane was above the 10% uncertainty of the concentration detected in the experimental blank (S5).

3.4 H_2 production estimated by Fe(III)/Fe(II) analysis

As previously stated, hydrogen is produced via the oxidation of Fe^{2+} in the starting material according to equation 4 (section 2.3.4). Therefore, the difference between the amounts of FeO measured in the starting material and the reaction products quantifies the Fe^{2+} that has been oxidized at high pressure and high temperature.

The analysis shows that the starting mine tailings sample contained, 1.3 mmol/g of FeO, whereas the reaction products of MT1, MT2 and MT4 experiments contained 1.3, 1.1 and 0.8 mmol/g of FeO, respectively. According to this result, the initial mine tailings and the MT1 experiment contained the same amount of FeO, meaning that no Fe^{2+} oxidation took place. However, 20 µmol/g of hydrogen was detected in the gas chromatography analysis of this experiment. This could possibly suggest an analytical error in detecting such a low level of FeO quantity due to the detection limit of the method used. The H_2 production estimated from the stoichiometric ratio with Fe^{3+} (given in eq. 4) are reported in Table 3 for the three experimental runs. Except for MT1, the estimated values of hydrogen are in good agreement with those observed in gas chromatography analysis.

Moreover, if all the Fe^{2+} in initial mine tailings (i.e. 1.3 mmol/g) was to completely oxidize into Fe^{3+}, then following the equation 4 (1 mole of H_2 produced for 2 moles of Fe^{2+} oxidized), it could produce 655 µmol of H_2 per one gram of mine tailings. This value can be used to calculate the reaction progress with respect to Fe oxidation in the system. Although the value for MT1, as mentioned earlier, is too low and thus unreliable to be properly exploited, the estimation shows that MT2 and MT4 reach 17.6 % and 40.5% completion of reaction respectively (see Table 3).

4. Discussion

4.1 Preferential dissolution of olivine within mine tailings at 473-573 K and 15-30 MPa

The suitability of geological material as carbon sequestration and hydrogen production feedstocks depends primarily on their reactivity and chemical composition (Power et al., 2013). Mafic and ultramafic rocks are rich in Ca^{2+}, Mg^{2+} and Fe^{2+}, and therefore, are the ideal sources for this purpose. New Caledonian mine tailings contained abundant Mg^{2+} and Fe^{2+}, and thus their chemical composition and reactivity favored CO_2 sequestration and hydrogen production. Mineral dissolution, is essentially the first step that makes Mg^{2+} and Fe^{2+} available for both carbonation and hydrogen production reactions, and is a function of crystal chemistry, particle size of reacting mineral, pH, and temperature. As shown in Figure 2, olivine dissolved gradually with increasing temperature of our experiments, indicating that for our grain sizes and pH, increasing temperatures were favoring the dissolution of olivine. Inevitably, XRD pattern does not indicate the dissolution of glass due to its lack of crystallinity. In acidic to neutral pH, the dissolution kinetics of olivine have been reported to be faster than that of basaltic glass, which is an approximation that can be made for mine tailings (Gudbrandsson et al., 2011; Wolff-Boenisch et al., 2006; Wolff-Boenisch et al., 2011). These two previous studies suggest that, under acidic conditions such as those of our study, the constituent minerals of crystalline basalt dissolve faster than basaltic glass by more than one order of magnitude (olivine, a nesosilicate with a Q_0 structure, has all silicate tetrahedrons disconnected from each other, as opposed to glass, and thus faster dissolution kinetics). This indicates that olivine is the major contributor to the Mg^{2+} and Fe^{2+} cations in the solution.

4.2 Reaction path and formation of secondary Mg-silicates

The XRD patterns of the products indicated that the reaction of mine tailings with CO_2-saturated water, resulted in Fe-rich magnesite, and small quantity of phyllosilicates.

Hydrogen is the gaseous product of this reaction. Hematite (Fe_2O_3) was observed only in MT4 (573 K/30 MPa) experiment. Although, we anticipated the production of hydrogen through serpentinization reaction, our result showed that the products of the reaction after 25 days consisted of smectites. However, formation of proto-serpentine-like phase using New Caledonian mine tailings was reported by Bodenan et al. (2014), in an experimental work where 1-day reactions took place either in water or in a 0.43 M NaCl/0.27 M $NaHCO_3$ solution at 453 K at a pCO_2 of 1-9 MPa.

The difference between the reaction products of those two sets of experiments cannot be explained by different pH conditions, as Bodénan et al.(2014) run experiments both in bicarbonate solution (which has the buffer ability to remain neutral under pCO_2 pressure), and in deionized water (which becomes acidic). The temperature, though lower in Bodénan et al.'s study (453K), remains close to our study's conditions (473-573K), and grain size (which influences specific surface area) should not have a critical influence on thermodynamic equilibrium. With respect to these parameters, the two studies are comparable, while their reaction products differ. One possible explanation could very well lie in the duration of the experiments. A study investigating the genesis of ultramafic hosted magnesite vein deposits by Abu-Jaber and Kimberly (1992) has reported, within natural samples, on the reaction of serpentine, magnetite and bicarbonate into (Fe-)nontronite (smectite) and magnesite. Furthermore, a recent experimental study describes various pathways for the conversion of serpentine to smectite under hydrothermal conditions, during which Al^{3+} substitutes to Si^{4+}. They suggest that solid-state transformation is the main mechanism involved. Since this is a process is kinetically limited, the difference in the experiments duration (1 day for Bodénan et al. vs 25 days for this study) could explain the different reaction product. Serpentine would therefore only be an intermediate phase.

4.3 Fe-rich magnesite precipitation and hydrogen production

Fe-rich magnesite was the only carbonate precipitated in our experiments as confirmed by XRD and Rock-Eval 6 analysis. Theoretically, mine tailings could precipitate a maximum of 77 wt.% of magnesite, assuming 100% dissolution of mine tailings (S11). The quantities of Fe-rich magnesite precipitated at 473 K/15 MPa, 523 K/30 MPa and 573 K/30 MPa were 20.3, 44.9 and 21.6 wt.%, respectively. If the reaction completion (Rx) with respect to carbonate precipitation is given by the ratio between the observed carbonate wt.% versus the calculated maximum carbonate wt.%, then 26.4%, 58.3% and 28.1% of reaction completion were achieved respectively during the experiments. Interestingly, the iron content in magnesite followed the same trend as reaction completion, with 0.08, 0.58 and 0.17 moles of iron in one mole of magnesite at 473 K/15 MPa, 523 K/30 MPa and 573 K/30 MPa respectively. This would indicate that the lower temperature and low pCO_2 in MT1 (473 K/15 MPa) slowed down kinetics of the dissolution and precipitation reactions resulting in low quantities of magnesite with small quantity of iron, compared to the other two experiments. The MT2 and MT4 experiments, which were conducted at same pCO_2 (30 MPa), revealed that almost all the olivine dissolved at increasing temperature up to 573 K. But, the precipitated magnesite at 523 K was twice higher than at 573 K. As Mg is the major element in magnesite, this result clearly indicates the competition of Mg incorporation into magnesite vs. secondary Mg-silicates in the 523-573 K temperature range. In addition, the quantity of iron incorporated in magnesite at 523 K is twice as high than at 573 K, indicating that temperatures between 523 -573K favored the incorporation of iron into other phases than magnesite. As shown by Andreani et al. (2012), the fast precipitation of Al-Fe-rich serpentines indeed competes with magnetite nucleation and may indeed inhibit it altogether. Nevertheless, magnetite formation is enhanced with increasing temperature, as shown by Malvoisin et al., 2012); those studies thus support the present observations and findings on Fe(III)

incorporation into secondary phases. Total iron (II+III) incorporation into secondary phases and its correlation with hydrogen production is also worth mentioning because it demonstrates the competition between two other reactions in the system: the iron incorporation into magnesite versus secondary Mg-silicates (±iron oxides). As the temperature increased from 523 K to 573 K, hydrogen production was approximately doubled, producing more Fe^{3+}. At 523 K, the most likely secondary phase to host Fe^{3+} was secondary phyllosilicate, whereas at 573 K, it could possibly be incorporated into phyllosilicate and into iron (III) oxides as well. Although, ferric-hydrate complexes could host Fe^{3+} ions, we assumed their quantities to be negligible. Magnesite structure accommodates only Fe^{2+}. Therefore, the results clearly indicate that temperatures between 523 -573K favor iron oxidation, whereas temperatures between 473 K and 523 K favor the iron incorporation into magnesite. The competition between Mg and Fe incorporation among the secondary phases seems to control the quantities of magnesite precipitation and hydrogen production. Moreover, Figure 5, which shows the magnesite production (in wt.%) versus hydrogen production clearly demonstrates that temperatures between 523 K and 540 K at pCO_2=30 MPa (shown by shaded area) would be the most favorable conditions for reacting mine tailings in order to maintain both carbonation and hydrogen production in significant quantities. Although the P/T conditions of maximum carbonation in our experiments differ slightly from those of Gerdermann et al. (2007), it can be argued that this discrepancy arises from the different solutions used in two studies; a CO_2-saturated water here compared with a 0.64M $NaHCO_3$, 1M NaCl solution in Gerdermann et al. (2007). Furthermore, Andreani et al. (2012) and Sissmann et al. (2013) mention the effect of aluminum on dissolution kinetics of olivine dissolution kinetics. Its presence in the associated glass phase of the mine tailings could also slightly change not only those dissolution kinetics but also the precipitation kinetics of carbonates.

483 The analysis of FeO in the starting material and the products were used to evaluate
484 the amount of iron oxidation, and to further confirm the hydrogen amounts measured by gas
485 chromatography. As mentioned in section 3.4, the Fe(III) / Fe(II) analysis of non-reacted mine
486 tailings confirmed that the starting material does not contain any Fe^{3+} that could have resulted
487 from ore processing. Assuming the mine tailings have been well homogenized after crushing
488 and sieving, the Fe^{2+} measured in the experimental products was expected to be lower than in
489 the initial sample, due to the oxidation of Fe^{2+} during the experiment. However, the amount of
490 Fe^{2+} measured for MT1 is slightly above the value measured for the initial non-reacted
491 sample. Such an inconsistency could be explained by potential inhomogeneities caused by a
492 sampling bias of the starting material or the products, or due to detection limit for low Fe
493 concentrations in this sample. Nevertheless, the estimated hydrogen production from MT2
494 and MT4 experiments are in good agreement with the measured hydrogen quantities using gas
495 chromatography (Table 3).

496 The variation of hydrogen production as a function of reaction time (Figure 4)
497 indicates that the hydrogen production at 473 K/15 MPa and 523 K/ 30 MPa continued to
498 increase steadily until the end of the experiment, whereas at 573 K/30 MPa, it suddenly
499 decreased after 9 days of reaction, reaching a plateau. This result suggests that at the lower
500 temperatures, the production on of H_2 is not buffered by new secondary phases (no
501 phyllosilicates passivating the surface of mine tailings). However, at 573K, it appears that
502 hydrogen production is being buffered. A possible explanation would be the limitation of Fe^{2+}
503 supply, and thus of further water reduction and H_2 production. Nevertheless, the sharp
504 decrease in H_2 concentration followed by a plateau could indicate that a steady state has been
505 reached, and that H_2 is being consumed to form light organic compounds dissolved within the
506 system (not quantified in this study) through a reaction with CO_2.

507

4.4 Carbonation and hydrogen production from mine tailings vs. other slags

First our results on CO_2 sequestration were compared with two experimental studies by Bobicki et al. (2015) and Garcia et al. (2014), who conducted experiments at T~423 K and PCO_2 ~15 MPa. Bobicki et al. (2015) used chrysotile from two nickel (Ni) mines (Okanogan nickel deposit in Washington State, USA (OK ore) and Thompson Nickel Belt in Manitoba, Canada, (Pipe ore), respectively) (table 4). The ores contained 6.0 and 7.8 wt.% of MgO, with approximately <7 wt.% of CaO+FeO. In contrast, Garcia et al. (2010) used pure olivine (Fo91), with 55.5 wt.% of MgO (theoretical), which is also close to the average MgO content of this study (53.6 wt.%), but containing nearly half of the iron compared to mine tailings in this study (12.95 wt.%). Our results on carbonation yields lie within the same order of magnitude compared to the two studies considered here. However, despite the large granulometry of the starting materials, Bobicki et al. (2015) was able to store CO_2 at a higher rate (~200 g/kg CO_2 within one hour) than the other two studies. They reacted olivine (formed from the reversion of heat-treated chrysotile) at the conditions previously suggested by Gerdemann et al. (2007), making solution salinity and bicarbonate concentration the main differences with the other two studies. This suggests that the rate of CO_2 storage in our experiments could have been enhanced if such high concentrations had been used. However, even though the rate was slower, MT2 experiment stored more CO_2 compared to Bobicki et al. (2015) and Garcia et al. (2010).

It is highly probable that the higher temperature range presumably limits carbonation, while the lower range limits H_2 production. The higher temperatures increase dissolution kinetics, leading to a larger amount of silica in solution. As that silica precipitates, they form secondary phyllosilicates that scavenge the divalent cations (equation 3). In contrast, the lower temperatures create lower silica supersaturation, and the cations enter carbonate phases leaving less iron available for oxidation and hydrogen production (equation

2). Nevertheless, this study proves that intermediate conditions can be set to make both processes work simultaneously.

The amounts of hydrogen produced in our experiments were compared with two similar studies (Crouzet et al., 2017; Malvoisin et al., 2013), who attempted to produce hydrogen by using pure wüstite (FeO) and Fe-rich steel slag (Table 5). For the sake of comparison, hydrogen produced at 473 K or 573 K, and 30 MPa after ca. 69 or 160 hours of each study were used. The study by Malvoisin et al. (2013) used a carbonated basic oxygen furnace (CARBOF) containing 2.7 wt.% Fe(0), 20.58 wt.% FeO and 3.16 wt.% Fe_2O_3. The grain size of original steel slag used for carbonation was 1 -50 µm. The second study (Crouzet et al., 2017) is a follow-up study of Malvoisin et al. (2013) that investigates the hydrogen production under acidic pH conditions using 50-100 µm size pure wüstite (FeO). Because the chemical composition of steel slag, wüstite and New Caledonian mine tailings largely differ from each other, we calculated the hydrogen production per mass unit of FeO of each material. In our study, the hydrogen measured by gas chromatography, and average FeO in mine tailings (12.95 wt.%) were used for this calculation.

As shown in Table 5, H_2 production seems to be correlated with pH: the lower it is, the higher the amount of H_2 generated. This can be explained by the fact that low pH promotes mineral dissolution and thus Fe^{2+} release. Thus, at a similar temperature (573K), this study (pH 3.9) generates more H_2 than Crouzet (pH 6.0), which generates more than Malvoisin (pH 6.9). However, the pH effect is not the only way to increase H_2 production. As shown by Crouzet et al. (2017), the addition of organic ligands (such as acetic acid) can increase H_2 generation even further by promoting mineral dissolution.

4.5 Implications for CO_2 sequestration and hydrogen production in New Caledonian mining sites and other Ni mining sites

New Caledonia is the 11th largest Ni producer in the world, preceded by the United states, Australia, Brazil, Canada, China, Columbia, Cuba, Guatemala, Indonesia and Madagascar (U.S. Geological Survey, 2017). When scaled to land area, however, its production of Nickel is in the top 3, implying a high environmental fingerprint. In 2013, New Caledonia produced 127,027 metric tons (t) of nickel from 7.8 million metric tons (Mt) of saprolite ore and 36,839 t of nickel from 4.2 Mt of laterite ore, resulting approximately in 12 million metric tons (Mt) of mine tailings per year (Wacaster 2013). The management of mine tailings such as collection, storage and re-usage are costly to process. Currently these mine tailings are used for geo-technical aspects such as building roads, dams, and land filling. Compared to the traditional valorization methods, those proposed by this study are novel and might be used to contribute to today's always-increasing energy demands, by producing an energy source through waste recycling. In addition, implementing a simultaneous ex-situ CO_2 storage and hydrogen production plant in the vicinity of mining sites provides a safe and permanent disposal of CO_2 emitted by the nickel industry. Although the chemical looping processes have been documented for carbon capture and storage (Bui et al., 2018; Cormos, 2017), the idea of energy looping does not appear prominently in literature. It is nevertheless our belief that inspiration could be drawn from chemical looping: the energy needed for heating the material could be obtained passively by locating this plant near high temperature furnaces used for ore-processing.

The annual CO_2 emission of New Caledonia is about 4.3 Mt/y (Boden et al., 2017). Our experiments having shown that at 523 K and 30 MPa, mine tailings can trap at least 320 g of CO_2 per kg of mine tailings (supporting information S6), it follows that the

annual mine tailings production could potentially trap 3.8 Mt/y of CO_2, which represents about 90% of New Caledonia's annual emissions.

The annual electrical consumption of New Caledonia is approximately 2400 GWh; (New Caledonia Department of Energy, 2013). The maximum hydrogen production in our experiments was 0.57 g hydrogen per kg of mine tailings at 573 K and 30 MPa. According to this value, the annual mine tailings produced in New Caledonia is able to produce 6840 tons of hydrogen per year, which is equivalent of generating 229 GWh/y (with H_2 combustion generating around 120.5 MJ/kg or 33.5 kWh/kg). It represents around 10 % of New Caledonia's annual electrical consumption. Furthermore, assuming an average family consumes 3400 kWh/y (New Caledonia Department of Energy, 2013), the energy produced would be sufficient to sustain around 67350 families.

One limiting factor regarding this method is the separation of small quantities of hydrogen from CO_2 in the reactor. Separating CO_2 and H_2 from industrially important gas mixtures (synthesis gas or natural gas) are widely performed using membrane methods (Korelskiy et al., 2015). These membranes could be either made from polymers (Ghadimi et al., 2014; Rabiee et al., 2014), or ceramic (Korelskiy et al., 2015), and they provide cost effective means of separating gases in large scale. In our opinion, a membrane method would be suitable to separate hydrogen from CO_2 in this process.

We believe that the simultaneous application of ex-situ CO_2 sequestration and hydrogen production using New Caledonian mine tailings could be easily applied to various mining industries of mafic rocks, which presumably produce mine wastes of similar compositional and mineralogical characteristics. By using the residual heat provided by a third process such as the high temperature smelting of ore, those two processes could be translated into a high-value, cost-effective industrial way of storing wastes and generating clean energy.

5. Conclusions

Batch experiments conducted between 473 K - 573 K under high pCO_2 of 15-30 MPa have demonstrated the viability of using New Caledonian mine tailings in ex-situ carbonation process, while producing H_2 as a byproduct. The results suggest that mine tailings were altered into Fe-rich magnesite and phyllosilicates when reacted with CO_2-saturated water at the above mentioned conditions. We have outlined that the competition between Mg and Fe incorporation among the secondary phases seems to control the quantities of magnesite precipitation and hydrogen production. Taken together, these results suggest that the temperatures between 523 K and 540 K at pCO_2=30 MPa would be the most favorable conditions for reacting mine tailings in order to maintain both carbonation and hydrogen production in significant quantities.

This work suggest a method to treat New Caledonia's annual CO_2 emissions and energy demands cost-efficiently by recycling the heat used in metal extraction (>1273 K), providing a novel valorization method for New Caledonian mine tailings. This approach can be globally applied to nickel (Ni) mine tailings as well as other industrial waste materials containing Ca, Mg, and Fe; however we believe that the optimum P/T conditions might vary depending on the mineral composition and textural features of individual material.

Acknowledgments

We thank Joel Lopes-Azvedo, Fanny Lutz, Julien Labaume for their support in mineralogical analysis. We also thank Daniel Pillot for his support in Rock-Eval 6 analysis. Virgile Rouchon, François Guyot and Valerie Beaumont are warmly acknowledged for their constructive comments and discussions. Finally, the thorough

review and constructive comments of the executive editor Prof. Michael Kersten and the two anonymous reviewers are greatly appreciated.

References

Abu-Jaber, N.S., Kimberley, M.M., 1992. Origin of ultramafic-hosted vein magnesite deposits. Ore Geol. Rev. 7, 155–191. doi:10.1016/0169-1368(92)90004-5

Allen, D.E., Seyfried, W.E., 2003. Compositional controls on vent fluids from ultramafic-hosted hydrothermal systems at mid-ocean ridges: An experimental study at 400° C, 500 bars. Geochim. Cosmochim. Acta. 67, 1531–1542. doi:10.1016/s0016-7037(02)01173-0

Andreani, M., Daniel, I., Pollet-Villard, M., 2012. Aluminum speeds up the hydrothermal alteration of olivine. Am. Mineral. 98, 1738–1744. doi:10.2138/am.2013.4469

Barnes, C.S and Koretsky, M.., 2004. In engineering and chemical thermodynamics. John Willey and Sons.

Béarat, H., McKelvy, M. J., Chizmeshya, A. V., Gormley, D., Nunez, R., Carpenter, R. W., ... & Wolf, G. H. (2006). Carbon sequestration via aqueous olivine mineral carbonation: role of passivating layer formation. Environmental science & technology, 40(15), 4802-4808.

Behar, F., Beaumont, V., De B. Penteado, H.L., 2001. Rock-Eval 6 technology: Performances and developments. Oil Gas Sci. Technol. 56, 111–134. doi:10.2516/ogst:2001013

Berndt, M.E., Allen, D.E., Seyfried, W.E., 1996. Reduction of CO_2 during serpentinization of olivine at 300°C and 500 bar. Geology. 24, 351–354. doi:10.1130/0091 7613(1996)024<0351:ROCDSO>2.3.CO

Bish, D.L., Howard, S.A., 1988. Quantitative phase analysis using the Rietveld method. J. Appl. Crystallogr. 21, 86–91. doi:10.1107/S0021889887009415

Bish, D.L., Post, J.E., 1993. Quantitative mineralogical analysis using the Rietveld full-pattern fitting method. Am. Mineral. 78(9-10), 932-940.

Bobicki, E.R., Liu, Q., Xu, Z., Zeng, H., 2012. Carbon capture and storage using alkaline industrial wastes. Prog. Energy Combust. Sci. doi:10.1016/j.pecs.2011.11.002

Bobicki, E. R., Liu, Q., & Xu, Z. (2015). Mineral carbon storage in pre-treated ultramafic ores. Minerals Engineering, 70, 43-54.

Boden, T, Marland, G, and Andres, R., 2017. Global, Regional, and National Fossil-Fuel CO_2 Emissions. Oak Ridge 3 National Laboratory, U.S. Department of Energy, Oak Ridge, Tenn., U.S.A.

Bodénan, F., Bourgeois, F., Petiot, C., Augé, T., Bonfils, B., Julcour-lebigue, C., Guyot, F., 2014. Ex situ mineral carbonation for CO_2 mitigation : Evaluation of mining waste resources, aqueous carbonation processability and life cycle assessment (Carmex project) 59, 52–63. doi:10.1016/j.mineng.2014.01.011

Brantley, S. L. (2003). Reaction kinetics of primary rock-forming minerals under ambient conditions. Treatise on geochemistry, 5, 605.

Brunauer, S., Emmett, P.H., Teller, E., 1938. Adsorption of Gases in Multimolecular Layer. J. Am. Chem. Soc. 60, 309–319. doi:citeulike-article-id:4074706

Bui, M., Adjiman, C. S., Bardow, A., Anthony, E. J., Boston, A., Brown, S., ... & Hallett, J. P. (2018). Carbon capture and storage (CCS): the way forward. Energy & Environmental Science.

Caesar, L., Rahmstorf, S., Robinson, A., Feulner, G., & Saba, V. (2018). Observed fingerprint of a weakening Atlantic Ocean overturning circulation. Nature, 556(7700), 191.

Cormos, C. C. (2011). Hydrogen production from fossil fuels with carbon capture and storage based on chemical looping systems. International journal of hydrogen energy, 36(10), 5960-5971.

Crouzet, C., Brunet, F., Recham, N., Findling, N., Lanson, M., Guyot, F., Ferrasse, J.H., Goffé, B., 2017. Hydrogen production by hydrothermal oxidation of FeO under acidic conditions. Int. J. Hydrogen Energy 42, 795–806. doi:10.1016/j.ijhydene.2016.10.019

Daval, D., Martinez, I., Corvisier, J., Findling, N., Goffé, B., Guyot, F., 2009a. Carbonation of Ca-bearing silicates, the case of wollastonite: Experimental investigations and kinetic modeling. Chem. Geol. 262, 262–277. doi:10.1016/j.chemgeo.2009.01.022

Daval, D., Martinez, I., Guigner, J. M., Hellmann, R., Corvisier, J., Findling, N., ... & Guyot, F. 2009b. Mechanism of wollastonite carbonation deduced from micro-to nanometer length scale observations. American Mineralogist, 94(11-12), 1707-1726.

Ece, Ö.I., Matsubaya, O., Çoban, F., 2005. Genesis of hydrothermal stockwork-type magnesite deposits associated with ophiolite complexes in the Kütahya-Eskişehir region, Turkey. Neues Jahrb. für Mineral. - Abhandlungen 181, 191–205. doi:10.1127/0077-7757/2005/0014

Edenhofer, O., Pichs-Madruga, R. Sokona, Y., Farahani, E., Kadner, S., Seyboth, K., Adler, A., Baum, I., Brunner, S., Eickemeier, P., Kriemann, B., Savolainen, J., Schlömer, S., von Stechow, C., Zwickel, T., Minx, J.C., 2014. IPCC, 2014. Summary for policymakers, climate change 2014: mitigation of climate change. Contribution of working group iii to the fifth assessment report of the intergovernmental panel on climate change. doi:10.1007/s13398-014-0173-7.2

Garcia, B., Beaumont, V., Perfetti, E., Rouchon, V., Blanchet, D., Oger, P., Dromart, G., Huc, A.Y., Haeseler, F., 2010. Experiments and geochemical modelling of CO_2 sequestration by olivine: Potential, quantification. Appl. Geochemistry 25, 1383–1396. doi:10.1016/j.apgeochem.2010.06.009

Gerdemann, S.J., O'Connor, W.K., Dahlin, D.C., Penner, L.R., Rush, H., 2007. Ex situ aqueous mineral carbonation. Environ. Sci. Technol. 41, 2587–2593. doi:10.1021/es0619253

Ghadimi, A., Amirilargani, M., Mohammadi, T., Kasiri, N., Sadatnia, B., 2014. Preparation of alloyed poly(ether block amide)/poly(ethylene glycol diacrylate) membranes for separation of CO_2/H_2(syngas application). J. Memb. Sci. 458, 14–26. doi:10.1016/j.memsci.2014.01.048

Golubev, S. V., Pokrovsky, O. S., & Schott, J. (2005). Experimental determination of the effect of dissolved CO2 on the dissolution kinetics of Mg and Ca silicates at 25 C. Chemical Geology, 217(3-4), 227-238.

Gudbrandsson, S., Wolff-Boenisch, D., Gislason, S.R., Oelkers, E.H., 2011. An experimental study of crystalline basalt dissolution from 2pH11 and temperatures from 5 to 75°C. Geochim. Cosmochim. Acta. 75, 5496–5509. doi:10.1016/j.gca.2011.06.035

Guthrie, G. (2001). Geochemical aspects of the carbonation of magnesium silicates in an aqueous medium (No. LA-UR-01-1429). Los Alamos National Lab., NM (US).

Guyot, F., Daval, D., Dupraz, S., Martinez, I., Ménez, B., Sissmann, O., 2011. CO_2 geological storage: The environmental mineralogy perspective. Comptes Rendus Geosci. 343, 246–259. doi:10.1016/j.crte.2010.12.007

Harrison, A.L., Dipple, G.M., Power, I.M., Mayer, K.U., 2016. The impact of evolving mineral-water-gas interfacial areas on mineral-fluid reaction rates in unsaturated porous media. Chem. Geol. 421, 65–80. doi:10.1016/j.chemgeo.2015.12.005

Harrison, A.L., Power, I.M., Dipple, G.M., 2013. Accelerated carbonation of brucite in mine tailings for carbon sequestration. Environ. Sci. Technol. 47, 126–134. doi:10.1021/es3012854

Janecky, D.R., Seyfried, W.E., 1986. Hydrothermal serpentinization of peridotite within the oceanic crust: Experimental investigations of mineralogy and major element chemistry. Geochim. Cosmochim. Acta. 50, 1357–1378. doi:10.1016/0016-7037(86)90311-X

Ji, S., Zhu, J., He, H., Tao, Q., Zhu, R., Ma, L., ... & Zhou, J. (2018). Conversion of serpentine to smectite under hydrothermal condition: Implication for solid-state transformation. American Mineralogist, 103(2), 241-251.

Johnson, N. C., Thomas, B., Maher, K., Rosenbauer, R. J., Bird, D., & Brown Jr, G. E. (2014). Olivine dissolution and carbonation under conditions relevant for in situ carbon storage. Chemical Geology, 373, 93-105.

King, H. E., Plümper, O., & Putnis, A. (2010). Effect of secondary phase formation on the carbonation of olivine. Environmental science & technology, 44(16), 6503-6509.

Klein, F., Bach, W., Jöns, N., McCollom, T., Moskowitz, B., Berquó, T., 2009. Iron partitioning and hydrogen generation during serpentinization of abyssal peridotites from 15°N on the Mid-Atlantic Ridge. Geochim. Cosmochim. Acta. 73, 6868–6893. doi:10.1016/j.gca.2009.08.021

Klein, F., Bach, W., McCollom, T.M., 2013. Compositional controls on hydrogen generation during serpentinization of ultramafic rocks. Lithos. 178, 55–69. doi:10.1016/j.lithos.2013.03.008

Klein, F., Garrido, C.J., 2010. On Serpentinization and Mineral Carbonation of Serpentinite. In AGU Fall Meeting Abstracts. Am. Geophys. Union.

Kondo, M., Ichii, K., Patra, P. K., Canadell, J. G., Poulter, B., Sitch, S., ... & Saigusa, N. (2018). Land use change and El Niño-Southern Oscillation drive decadal carbon balance shifts in Southeast Asia. Nature communications, 9.

Lackner, K.S., Wendt, C.H., Butt, D.P., Joyce, E.L., Sharp, D.H., 1995. Carbon-dioxide disposal in carbonate minerals. Energy. 20, 1153–1170. doi:10.1016/0360-5442(95)00071-n

Lafargue, E., Marquis, F., Pillot, D., 1998. Rock-Eval 6 applications in hydrocarbon exploration, production, and soil contamination studies. Oil Gas Sci. Technol. 53, 421–437. doi:10.2516/ogst:1998036

Lugli, S., Torres-Rutz, J., Garuti, G., Olmedo, F., 2000. Petrography and geochemistry of the Eugui magnesite deposit (Western Pyrenees, Spain): evidence for the development of a peculiar zebra banding by dolomite replacement. Econ. Geol. 95(8), 1775-1791. doi:10.2113/gsecongeo.95.8.1775

Malvoisin, B., Brunet, F., Carlut, J., Montes-Hernandez, G., Findling, N., Lanson, M., Vidal, O., Bottero, J.Y., Goff, B., 2013. High-purity hydrogen gas from the reaction between BOF steel slag and water in the 473-673 K range. Int. J. Hydrogen Energy. 38, 7382–7393. doi:10.1016/j.ijhydene.2013.03.163

Malvoisin, B., Brunet, F., Carlut, J., Rouméjon, S., Cannat, M., 2012a. Serpentinization of oceanic peridotites: 2. Kinetics and processes of San Carlos olivine hydrothermal alteration. J. Geophys. Res. Solid Earth. 117, 1–13. doi:10.1029/2011JB008842

Malvoisin, B., Carlut, J., Brunet, F., 2012b. Serpentinization of oceanic peridotites: 1. A high-sensitivity method to monitor magnetite production in hydrothermal experiments. J. Geophys. Res. Solid Earth 117. doi:10.1029/2011JB008612

769 Manabe, S., Stouffer, R.J., 1993. Century-scale effects of increased atmospheric CO_2 on
770 the ocean-atmosphere system. Nature 364, 215–218. doi:10.1038/364215a0

771 Marcaillou, C., Muñoz, M., Vidal, O., Parra, T., Harfouche, M., 2011a. Mineralogical
772 evidence for H_2 degassing during serpentinization at 300°C/300bar. Earth Planet. Sci.
773 Lett. 303, 281–290. doi:10.1016/j.epsl.2011.01.006

774 Marzeion, B., Kaser, G., Maussion, F., & Champollion, N. (2018). Limited influence of
775 climate change mitigation on short-term glacier mass loss. Nature Climate Change, 8(4),
776 305.

777 Matter, J.M., Kelemen, P.B., 2009. Permanent storage of carbon dioxide in geological
778 reservoirs by mineral carbonation. Nat. Geosci. 2, 837–841. doi:10.1038/ngeo683

779 Matter, J.M., Stute, M., Hall, J., Mesfin, K., Snæbjörnsdóttir, S., Gislason, S.R., Oelkers,
780 E.H., Sigfusson, B., Gunnarsson, I., Aradottir, E.S., Alfredsson, H.A., Gunnlaugsson, E.,
781 Broecker, W.S., 2014. Monitoring permanent CO_2 storage by in situ mineral carbonation
782 using a reactive tracer technique, in: Energy Procedia. pp. 4180–4185.
783 doi:10.1016/j.egypro.2014.11.450

784 McCollom, T.M., Bach, W., 2009a. Thermodynamic constraints on hydrogen generation
785 during serpentinization of ultramafic rocks. Geochim. Cosmochim. Acta. 73, 856–875.
786 doi:10.1016/j.gca.2008.10.032

787 McCollom, T.M., Bach, W., 2009b. Thermodynamic constraints on hydrogen generation
788 during serpentinization of ultramafic rocks. Geochim. Cosmochim. Acta. 73, 856–875.
789 doi:10.1016/j.gca.2008.10.032

790 McCollom, T.M., Klein, F., Robbins, M., Moskowitz, B., Berquó, T.S., Jöns, N., Bach, W.,
791 Templeton, A., 2016. Temperature trends for reaction rates, hydrogen generation, and
792 partitioning of iron during experimental serpentinization of olivine. Geochim.
793 Cosmochim. Acta. 181, 175–200. doi:10.1016/j.gca.2016.03.002

794 McCollom, T.M., Seewald, J.S., 2001. A reassessment of the potential for reduction of
795 dissolved CO_2 to hydrocarbons during serpentinization of olivine. Geochim. Cosmochim.
796 Acta. 65, 3769–3778. doi:10.1016/S0016-7037(01)00655-X

797 McCusker, L.B., Von Dreele, R.B., Cox, D.E., Louër, D., Scardi, P., 1999. Rietveld
798 refinement guidelines. J. Appl. Crystallogr. 32, 36–50. doi:10.1107/S0021889898009856

799 McMollom, T.M., Bach, W., 2008. Constraints on hydrogen generationduring
800 serpentinization of ultramaficrocks. Geochim. Cosmochim. Acta 72, A611.

801 New Caledonia Department of Energy, 2013. Bilan energetique de la nouvelle-caledonie-
802 2013. Retrieved from https://maitrise-
803 energie.nc/sites/default/files/documents/bilan_energetique_2013.pdf

NOAA, 2016. Trends in Atmospheric Carbon Dioxide. Retrieved from http://www.esrl.noaa.gov/gmd/ccgg/trends/.

O'Connor, W. K., Dahlin, D. C., Turner, P. C., & Walters, R. P. 2000. Carbon dioxide sequestration by ex-situ mineral carbonation (No. DOE/ARC-1999-009). Albany Research Center (ARC), Albany, OR.

Oelkers, E.H., 2005. Geochemical aspects of CO_2 sequestration. Chem. Geol. 217, 183–186. doi:10.1016/j.chemgeo.2004.12.006

Oskierski, H.C., Dlugogorski, B.Z., Jacobsen, G., 2013. Sequestration of atmospheric CO_2 in a weathering-derived, serpentinite-hosted magnesite deposit: ^{14}C tracing of carbon sources and age constraints for a refined genetic model. Geochim. Cosmochim. Acta. 122, 226–246. doi:10.1016/j.gca.2013.08.029

Palinkaš, L.A., Jurković, I., Garašić, V., Palinkaš, S.S., 2012. Genesis of vein-stockwork cryptocrystalline magnesite from the dinaride ophiolites. Ofioliti. 37, 13–26.

Park, A. H. A., Jadhav, R., & Fan, L. S. (2003). CO2 mineral sequestration: chemically enhanced aqueous carbonation of serpentine. The Canadian Journal of Chemical Engineering, 81(3‐4), 885-890.

Power, I.M., Harrison, A.L., Dipple, G.M., Wilson, S.A., Kelemen, P.B., Hitch, M., Southam, G., 2013. Carbon Mineralization: From Natural Analogues to Engineered Systems. Rev. Mineral. Geochemistry 77, 305–360. doi:10.2138/rmg.2013.77.9

Rabiee, H., Soltanieh, M., Mousavi, S.A., Ghadimi, A., 2014. Improvement in CO_2/H_2 separation by fabrication of poly(ether-b-amide6)/glycerol triacetate gel membranes. J. Memb. Sci. 469, 43–58. doi:10.1016/j.memsci.2014.06.026

Seifritz, W., 1990. CO_2 disposal by means of silicates. Nature. 345(6275), 486. doi:10.1038/345486b0

Seyfried, W.E., Foustoukos, D.I., Fu, Q., 2007. Redox evolution and mass transfer during serpentinization: An experimental and theoretical study at 200°C, 500bar with implications for ultramafic-hosted hydrothermal systems at Mid-Ocean Ridges. Geochim. Cosmochim. Acta. 71, 3872–3886. doi:10.1016/j.gca.2007.05.015

Sissmann, O., Brunet, F., Martinez, I., Guyot, F., Verlaguet, A., Pinquier, Y., Daval, D., 2014. Enhanced olivine carbonation within a basalt as compared to single-phase experiments: Reevaluating the potential of CO_2 mineral sequestration. Environ. Sci. Technol. 48, 5512–5519. doi:10.1021/es405508a

Sissmann, O., Daval, D., Brunet, F., Guyot, F., Verlaguet, A., Pinquier, Y., Findling, N., Martinez, I., 2013. The deleterious effect of secondary phases on olivine carbonation yield: Insight from time-resolved aqueous-fluid sampling and FIB-TEM characterization. Chem. Geol. 357, 186–202. doi:10.1016/j.chemgeo.2013.08.031

Snæbjörnsdóttir, S., Oelkers, E.H., Mesfin, K., Aradóttir, E.S., Dideriksen, K., Gunnarsson, I., Gunnlaugsson, E., Matter, J.M., Stute, M., Gislason, S.R., 2017. The chemistry and saturation states of subsurface fluids during the in situ mineralisation of CO_2 and H_2S at the CarbFix site in SW-Iceland. Int. J. Greenh. Gas Control 58, 87–102. doi:10.1016/j.ijggc.2017.01.007

Takahashi, E., 1986. Melting of a dry peridotite KLB-1 up to 14 GPa: Implications on the Origin of peridotitic upper mantle. J. Geophys. Res. 91, 9367–9382. doi:10.1029/JB091iB09p09367

U.S. Geological Survey, 2017. Mineral Commodity Summaries 2017.

van der Lee, J and De Windt, L., 2002. CHESS tutorial and cookbook updated for version 3.0. Ecole des Mines de Paris, Fontainebleau, France.

Wacaster, S., 2013. Minerals Yearbook New Caledonia (advance release). U.S. Geological survey.

Wilson, S.A., Harrison, A.L., Dipple, G.M., Power, I.M., Barker, S.L.L., Ulrich Mayer, K., Fallon, S.J., Raudsepp, M., Southam, G., 2014. Offsetting of CO_2 emissions by air capture in mine tailings at the Mount Keith Nickel Mine, Western Australia: Rates, controls and prospects for carbon neutral mining. Int. J. Greenh. Gas Control. 25, 121–140. doi:10.1016/j.ijggc.2014.04.002

Wolff-Boenisch, D., Gislason, S. R., & Oelkers, E. H. (2006). The effect of crystallinity on dissolution rates and CO2 consumption capacity of silicates. Geochimica et Cosmochimica Acta, 70(4), 858-870.

Wolff-Boenisch, D., Wenau, S., Gislason, S. R., & Oelkers, E. H. (2011). Dissolution of basalts and peridotite in seawater, in the presence of ligands, and CO_2: Implications for mineral sequestration of carbon dioxide. Geochimica et Cosmochimica Acta, 75(19), 5510-5525.

Zhang, X., Knorr, G., Lohmann, G., & Barker, S. (2017). Abrupt North Atlantic circulation changes in response to gradual CO 2 forcing in a glacial climate state. Nature Geoscience, 10(7), 518.

Zedef, V., Russell, M.J., Fallick, A.E., Hall, A.J., 2000. Genesis of vein stockwork and sedimentary magnesite and hydromagnesite deposits in the ultramafic terranes of southwestern Turkey: A stable isotope study. Econ. Geol. 95, 429–445. doi:10.2113/gsecongeo.95.2.429

Supporting information for the manuscript entitled;

Simultaneous ex-situ CO_2 mineral sequestration and H_2 production from New Caledonian mine tailings

Kanchana Kularatne[a,b (*)], Olivier Sissmann[a],Eric Kohler[a], Michel Chardin[a], Sonia Noirez[a], Isabelle Martinez[b]

[a]IFP Energies Nouvelles, 1- 4 Avenue du Bois Préau, 92852 Rueil-Malmaison, France

[b]Institut de Physique du Globe de Paris, Sorbonne Paris Cité, Université Paris Diderot, UMR 7154 CNRS, 1 rue Jussieu, F-75005 Paris, France

Gas phase data

S1.The composition of gas phase of MT1 experiment conducted at 473 K and 15 MPa.

MT1					
Duration	**H2**	**CH4**	**CO2**	**N2**	**O2**
(days)	**(µmols/g)**	**(µmols/g)**	**(mmols/g)**	**(mmols/g)**	**(mmols/g)**
0.1	4.54	-	94.6	0.24	0.04
0.9	1.44	-	94.0	3.84	0.99
1.8	1.35	-	91.0	7.98	2.02
2.8	4.76	-	106.8	-	-
5.8	6.62	-	113.8	0.24	0.04
7.8	5.94	-	119.1	-	-
8.8	8.42	-	127.0	-	-
9.8	8.01	0.17	130.9	-	-
13.0	0.21	-	136.4	-	-
13.8	6.11	0.24	143.0	-	-
16.0	16.92	0.23	149.3	-	-
20.0	15.20	0.27	154.1	-	-
22.8	17.87	-	159.8	-	-
23.8	19.99	-	165.9	0.05	-

884 S2. The composition of gas phase of MT2 experiment conducted at 523 K and 30 MPa.

MT2									
Duration	**H2**	**CH4**	**CO2**	**N2**	**O2**	**C2H6**	**C3H8**	**iC4H10**	**nC4H11**
(days)	**(μmols/g)**	**(μmols/g)**	**(mmols/g)**	**(mmols/g)**	**(mmols/g)**	**(μmols/g)**	**(μmols/g)**	**(μmols/g)**	**(μmols/g)**
0.00	0.00	0.00	179.13	0.13	0.02	-	-	-	-
0.69	0.00	0.43	184.38	0.18	-	-	-	-	-
0.96	0.00	5.71	189.23	0.18	-	-	-	-	-
1.71	0.00	0.44	195.42	0.18	-	-	-	-	-
1.96	3.48	0.21	200.97	-	-	-	-	-	-
4.68	2.79	0.22	206.68	0.17	0.19	-	-	-	-
5.88	5.64	0.65	211.31	0.29	0.03	-	-	-	-
6.68	7.67	1.44	215.93	0.61	0.11	-	-	-	-
7.72	6.52	0.76	228.60	0.46	0.04	-	-	-	-
8.92	8.37	0.75	228.11	0.23	-	-	-	-	-
11.71	43.67	4.82	231.46	0.24	-	0.41	0.59	0.04	1.27
13.71	47.75	12.33	228.82	6.52	1.46	4.01	1.93	0.36	2.23
14.71	37.48	3.59	242.22	0.25	-	-	0.38	0.03	0.72
18.71	53.80	2.56	247.42	0.40	0.04	-	0.42	-	0.67
20.75	117.57	5.94	253.49	0.64	0.09	-	0.58	0.03	0.99
22.75	58.49	1.41	258.83	-	-	-	-	-	-
25.76	76.69	2.00	263.83	-	-	-	-	-	-

885

886

887

S3.The composition of gas phase of MT4 experiment conducted at 573 K and 30 MPa.

MT4									
Duration	**H2**	**CH4**	**CO2**	**N2**	**O2**	**C2H6**	**C3H8**	**iC4H10**	**nC4H11**
(days)	**(μmols/g)**	**(μmols/g)**	**(mmols/g)**	**(mmols/g)**	**(mmols/g)**	**(μmols/g)**	**(μmols/g)**	**(μmols/g)**	**(μmols/g)**
0	0.00	0.10	183.56	0.38	0.10	-	-	-	-
0.76	116.17	9.93	146.34	0.78	0.15	-	0.82	-	1.89
1.13	106.77	11.32	147.27	4.92	1.14	-	1.95	0.09	2.89
1.80	0.00	0.47	200.07	2.47	0.47	-	-	-	-
2.85	186.29	26.19	138.04	22.60	-	3.70	10.72	0.60	11.08
4.04	0.00	1.76	208.04	3.71	0.93	-	-	-	-
6.83	145.06	1.73	219.28	-	-	-	-	-	-
8.83	283.50	1.22	226.74	-	-	-	-	-	-
9.88	35.97	8.47	230.83	1.40	0.17	0.79	2.12	0.10	2.87
13.83	73.78	5.85	238.71	0.20	0.02	-	0.45	0.04	1.40
15.88	41.76	4.72	245.09	0.15	0.01	-	0.37	0.30	0.73
17.88	48.17	5.49	249.76	0.16	0.01	-	-	0.19	0.71
20.88	21.94	1.88	245.44	-	-	-	-	-	-
24.01	41.18	24.14	247.30	0.50	0.12	8.16	16.95	0.74	14.76

S4. The composition of gas phase of MT2b experiment conducted at 523 K and 30 MPa. This is a blank experiment conducted at similar PT conditions in comparison with MT2, without introducing mine tailings in the reactor (due to technical difficulties, CO2 was not readjusted after the first sampling).

MT2b									
Duration	**H2**	**CH4**	**CO2**	**N2**	**O2**	**C2H6**	**C3H8**	**iC4H10**	**nC4H11**
(days)	**(µmols/g)**	**(µmols/g)**	**(mmols/g)**	**(mmols/g)**	**(mmols/g)**	**(µmols/g)**	**(µmols/g)**	**(µmols/g)**	**(µmols/g)**
7.21	-	0.15	280.94	0.10	-	-	-	-	-
19.17	-	2.42	192.34	0.19	0.03	1.67	7.28	0.81	12.16
24.17	-	3.81	197.10	0.20	0.02	2.05	8.37	1.17	16.95

S5.The composition of gas phase of MT4b experiment conducted at 573 K and 30 MPa. This is a blank experiment without reactants in order to monitor H2 and CH4 concentrations. It was conducted at similar PT conditions in comparison with MT4, without introducing mine tailings in the reactor (due to technical difficulties, CO2 was not readjusted after the first sampling).

MT4b									
Duration	**H2**	**CH4**	**CO2**	**N2**	**O2**	**C2H6**	**C3H8**	**iC4H10**	**nC4H11**
(days)	**(µmols/g)**	**(µmols/g)**	**(mmols/g)**	**(mmols/g)**	**(mmols/g)**	**(µmols/g)**	**(µmols/g)**	**(µmols/g)**	**(µmols/g)**
7.21	-	7.44	280.58	-	-	2.51	6.02	0.30	7.30
19.17	-	7.76	191.52	0.33	0.16	6.72	26.92	3.55	52.42
24.17	-	7.49	195.13	0.29	0.13	4.29	13.39	1.84	28.87

Quantification of secondary phases

S6. Calculation of carbonate yield

The quantification of carbonate phases using Rock-Eval 6 (Behar et al., 2001) involves pyrolysis and oxidation of ~40 mg of sample in an inert gas flow above 400 °C and oxidation at temperatures between 650°C–850°C. The gaseous CO_2 produced during the pyrolysis and oxidation cycles is analyzed by an infra-red analyzer (eg; S3' peak and S5 peak respectively) in online mode and the peak areas of S3' and S5 peaks are used to calculate the percent weight of carbonate according to the equations,

PyroMinC (wt.%)= [[S3^'* 12/44]+[S3'CO/2]*12/28]/10

OxiMinC (wt.%)= [S5*12/44]/10

The amount of total mineral carbon (MinC) in the sample is obtained by the addition of weight percent (wt.%) of mineral carbon produced from pyrolysis cycle (PyroMinC) and oxidation cycle (OxyMinC) as below,

MinC (wt.%) = PyoMinC + OxyMinC

$wt\%_{Carbonate} = MinC \times (M_{carbonate} / M_{carbon})$, where the molar mass of carbon is 12 g/mol the molar mass of carbonates is :

- for MT1 M ($(Mg_{0.92}Fe_{0.08})CO_3$) = 86.8 g/mol
- for MT2 M ($(Mg_{0.58}Fe_{0.42})CO_3$) = 97.53 g/mol
- for MT4 M ($(Mg_{0.83}Fe_{0.17})CO_3$) = 89.7 g/mol

-

	MinC	M $_{carbonate}$ g/mol	wt% Carbonate	m $_{Carbonate}$ g/kg	n $_{Carbonate}$ mol/kg	n CO_2 mol/kg	m CO2 g/kg
MT1	2.8	86.8	20.3%	225.7	2.60	2.60	114.4
MT2	6.62	97.5	53.8%	710.5	7.28	7.28	320.5
MT4	2.89	89.7	21.6%	241.6	2.69	2.69	118.5

928 Calculations for the amount of CO_2 trapped can be performed as follows :

$$m_{CO2\ trapped} = \frac{M_{CO2}}{M_{carbonate}} \times m_{carbonate}$$

$$m_{CO2\ trapped} = \frac{M_{CO2}}{M_{carbonate}} \times (wt\%_{carbonate} \times m_{run\ products})$$

$$m_{CO2\ trapped} = \frac{M_{CO2}}{M_{carbonate}} \times wt\%_{carbonate} \times (m_{0\ mine\ tailings} + m_{CO2\ trapped})$$

929 e.g. for MT2 : $m_{CO2\ trapped} = \frac{44}{97.53} \times 53.8\,\% \times (2\ g + m_{CO2\ trapped})$

$$m_{CO2\ trapped} = 0.485\ g + (0.243 \times m_{CO2\ trapped})$$

$$m_{CO2\ trapped} = 0.485\ g + (0.243 \times m_{CO2\ trapped})$$

$$m_{CO2\ trapped} = 0.641\ g\ for\ 2\ g\ of\ mine\ tailings)$$

$$m_{CO2\ trapped} = 320\ g\ for\ 1\ kg\ of\ mine\ tailings$$

930

931

932

933

934

935

SEM analysis on reaction products

S7. SEM images of the ionically polished sections of experimental product at T = 473 K and P = 15 MPa showing large anhedral magnesite crystals grown around glass (gl) and olivine (ol). Secondary phyllosilicates (phy) layers around glass. (b) magnified image of yellow square marked on (a); (c) glass altered into magnesite; The chemical composition of phyllosilicate, magnesite, olivine and glass analyzed by SEM-EDX are shown in the pie charts.

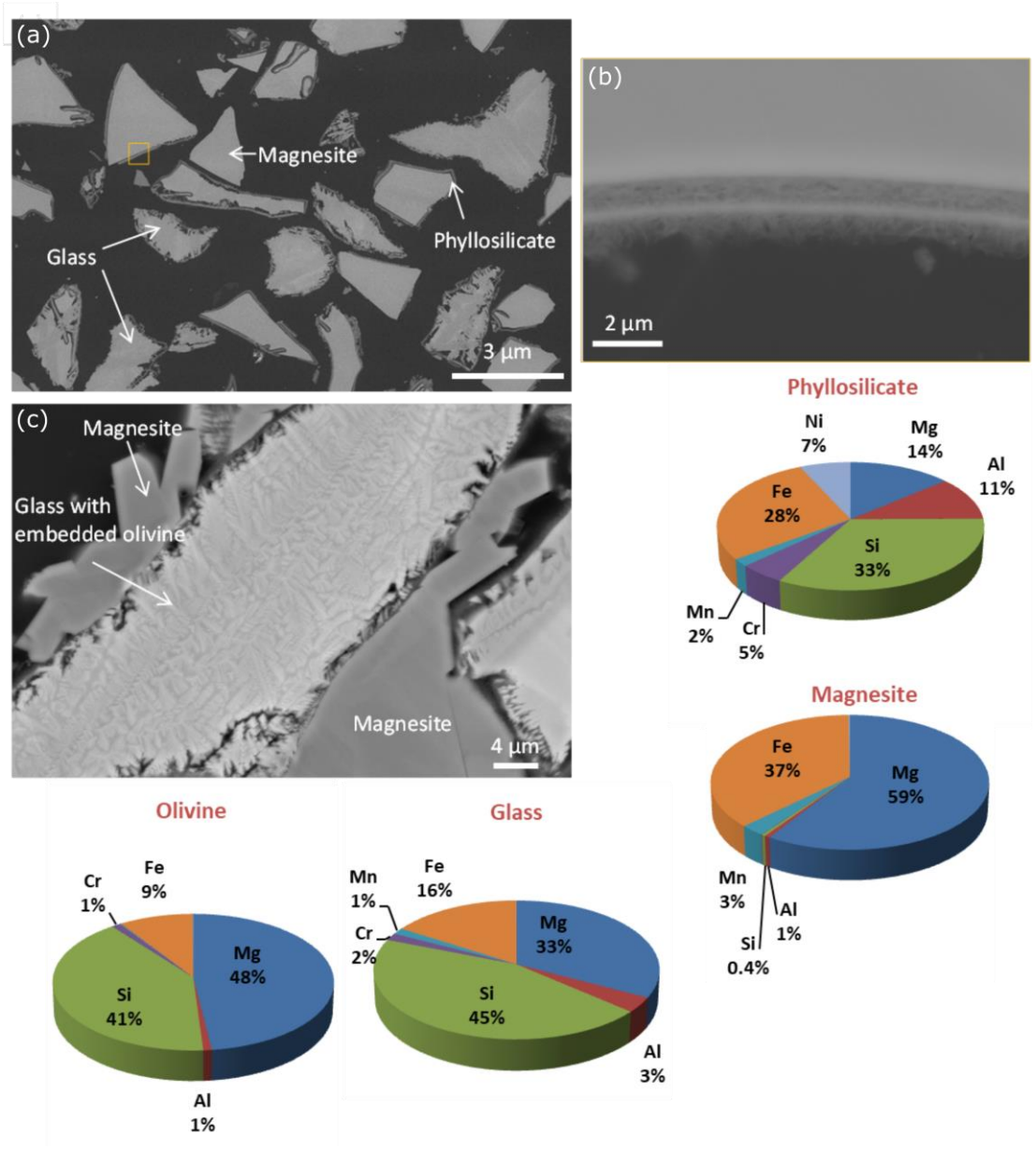

S8. SEM images of the ionically polished sections of experimental product at T = 523 K and P = 30 MPa showing euhedral magnesite crystals and secondary phyllosilicates. (b) a magnified view of phyllosilicate (c) SEM image of a polished section of the products showing magnesite with zoning. The chemical composition obtained by SEM EDX analysis is shown in pie charts.

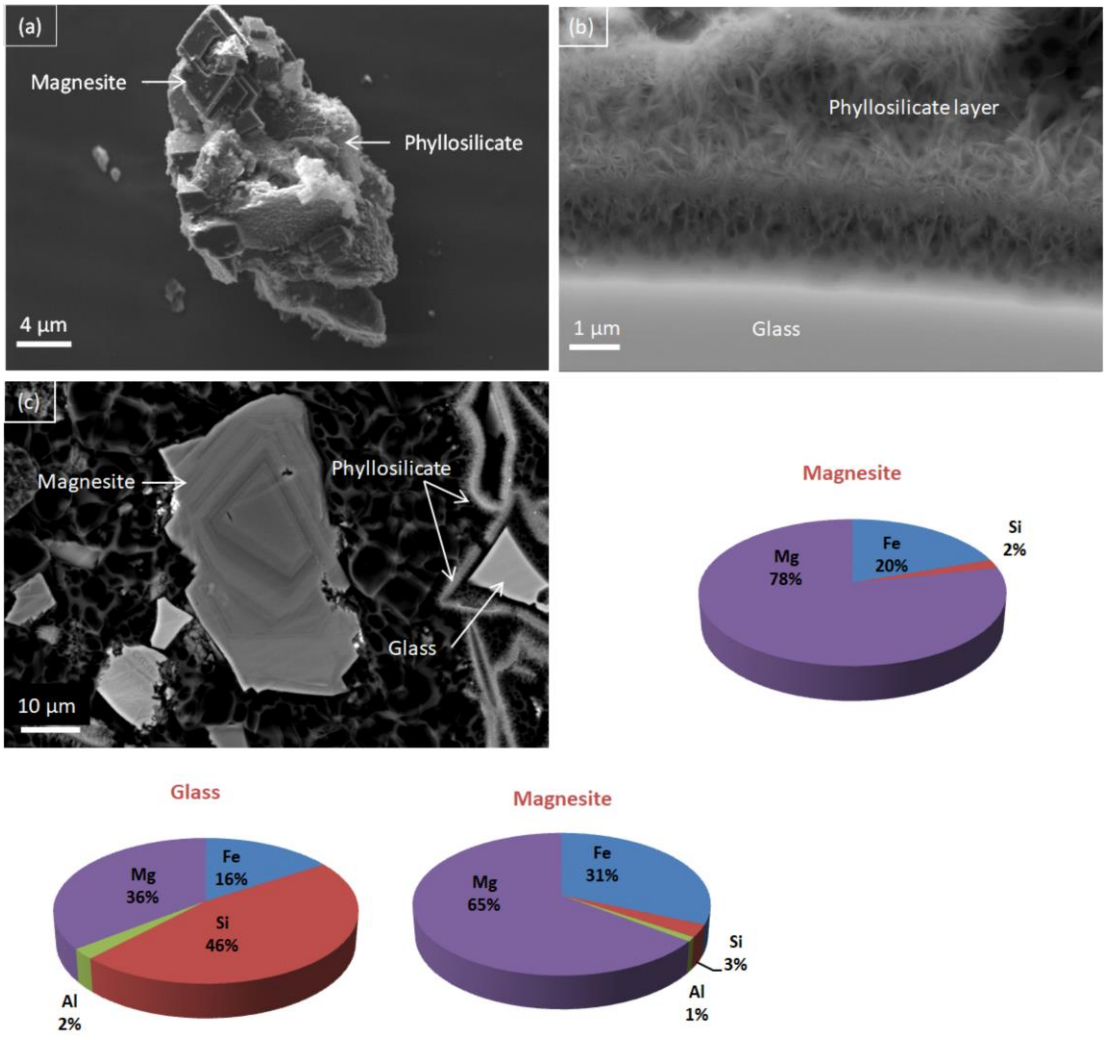

S9. SEM images of the ionically polished sections of experimental product at T = 573 K and P = 30 MPa, showing anhedral magnesite formed around glass, and heavily altered glass with thick layers of phyllosilicate.

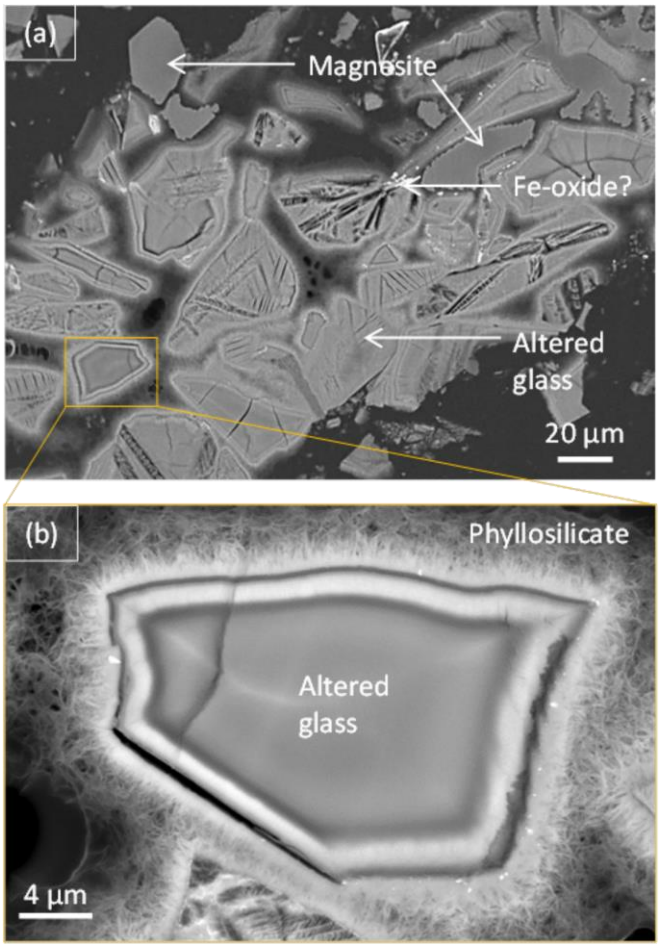

S10. FIB –TEM analysis

Ultra-thin, electron transparent (<200 nm) sections of each solid reaction product was prepared by performing FIB milling at IPGP and also at Institute of Electronics, Microelectronics and Nanotechnology (IEMN), Lille using a gallium (Ga) beam. These sections which are thinned down to electron transparency (<200 nm) were then analyzed using transmission electron microscopy (TEM). For this study, we only used the composition of magnesite obtained by the TEM-EDX analysis, and the detailed mineralogical analysis of other phases, in order to understand the mineral-water interactions, is still on going.

S11. Calculation of maximum carbonation of mine tailings

Fo88	molar mass		
(Mg1.76,Fe0.24)2SiO4	148.21	g/mol	
MgO1.76 + FeO0.24	88.16		
Mg(0.8)Fe0.2CO3	87.43	g/mol	
CO2	44	g/mol	45 wt.% Fo88
MgO1.76 + FeO0.24+2CO2	176.16		79.272
Olivine + 2CO2	236.21	g/mol	106.2954
Ratio max carbonation	**74.58%**		**74.58%**
glass			
(Mg1.50,Fe0.50)2SiO3	126.45	g/mol	
MgO1.50 + FeO0.50	82.4		
Mg(0.75)Fe0.25CO3	92.125	g/mol	55 wt.% glass
CO2	44	g/mol	93.72
(Mg1.50,Fe0.50)2SiO3+CO2	170.4		117.9475
GLASS + CO2	214.45	g/mol	**79.46%**
Ratio max carbonation	**79.46%**		
		Fo88+glass	Average
		MT composit	172.992
			224.2429
		Ratio max ca	**77.14%**

Figure 1. Powdered mine tailings observed under SEM (a) secondary electron image of powdered and cleaned sample used for the experiments. The grain surfaces are free of any adhered particles (b) angle selective back scattered image of a polished section of mine tailings showing the olivine crystals (white), embedded in glass (gray matrix) resulting a dendritic texture.

Figure 2. Mineralogical analysis of experimental run products (a) Element mapping (SEM) performed on a polished section the run product of experiment MT2 (T = 523 K and P = 30 MPa), showing formation of magnesite in large quantities (color coded by blue (Fe), green (Si) and red (Mg)). Magnesite crystals are shown in pink and initial silicate glass and traces of phyllosilicate is shown in green. A very small amount of iron oxide phases (not detectable through XRD) was observed only in this region of the sample and is marked in blue. (b) SEM secondary electron (In-lens detector) image of the same experimental run product taken on carbon coated powder showing euhedral grain of Fe-bearing magnesite (-as shown in SEM-EDX spectra) embedded in phyllosilicate. (c) X ray powder diffraction pattern of non-treated mine tailings sample and the run products of the three batch experiments, showing the progressive disappearance of olivine (O) peaks and the formation of magnesite (Mgs) during the reaction at high pressure and high temperature. The other secondary phases were phyllosilicates (Phy), and hematite (Hem). The peaks labeled (C) in the non-treated sample are the reflections of corundum which was added to the sample as the internal standard to quantify the fraction of glass (amorphous) in the initial non-reacted main tailings.

Figure 3. (a) SE image of the experimental run product at 473 K/15 MPa, showing some remaining glass, thin phyllosilicate layer formed around mine tailings and newly formed magnesite crystals; (b) a grain of mine tailing with olivine embedded in glass, which reacted to form anhedral magnesite crystals; (c) large magnesite crystals formed at 523 K/ 30 MPa showing Fe, Mg compositional zoning, and phyllosilicates which apparently detached from the original grains; (d) glass altered at 573 K/ 30 MPa forming a thick phyllosilicate layer.

Figure 4. Variations in the production of H_2, measured in the gas phase as a function of time (red points). The blue points represent blank experiments, which didn't yield any measurable concentrations of hydrogen. The error bars around the data points (smaller than the marker for most of them) represent a 5% uncertainty associated with the concentration measurements of hydrogen (H_2) by gas chromatography.

Figure 5: Quantities of magnesite precipitation and hydrogen production, obtained during the reaction of New Caledonian mine tailings, with CO_2-saturated water and as a function of temperature. The diagram emphasizes the competition between the two reactions. The shaded area indicates the temperature range at 30 MPa, recognized as the best conditions for the simultaneous carbonation and hydrogen production from mine tailings.

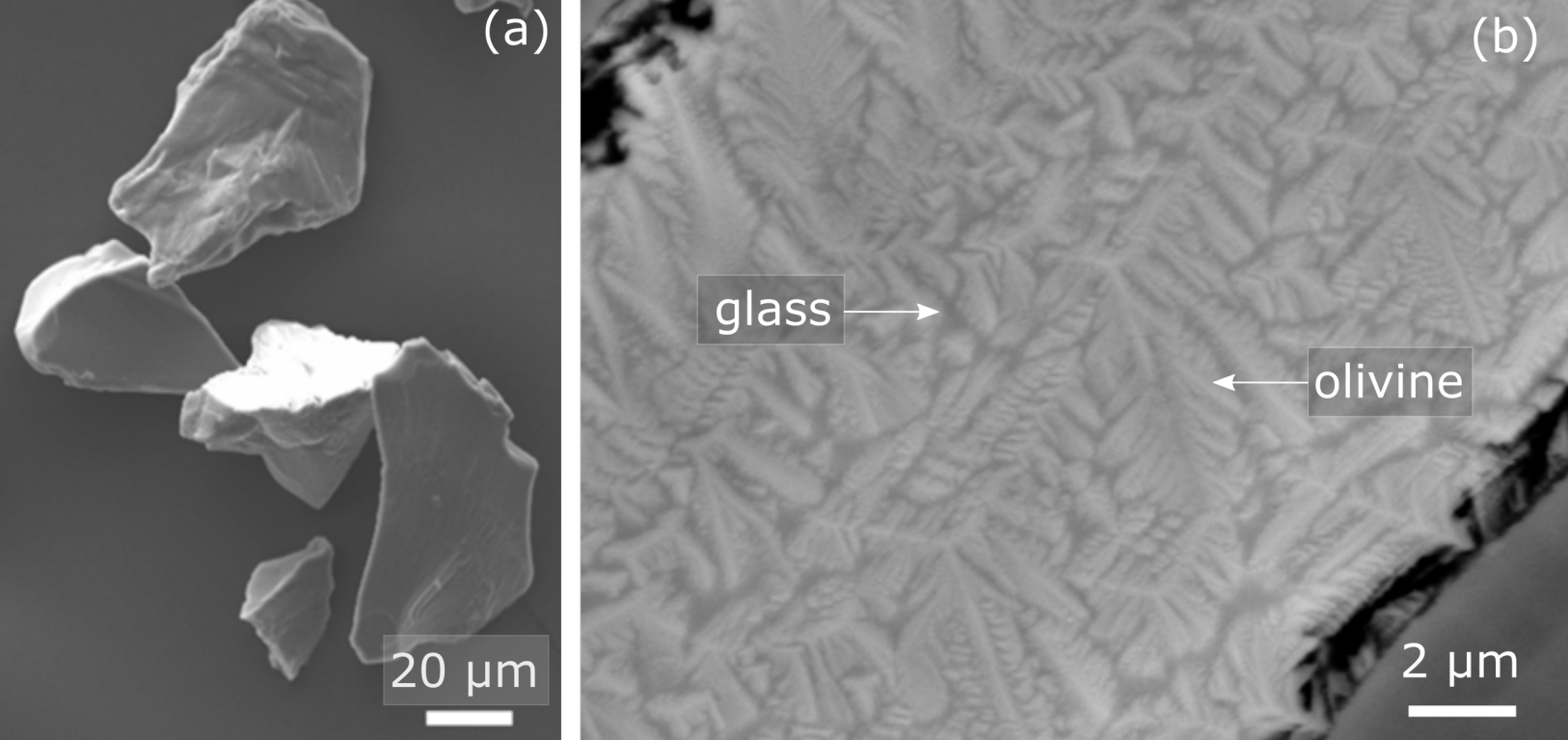
(a)
20 µm
(b)
glass
olivine
2 µm

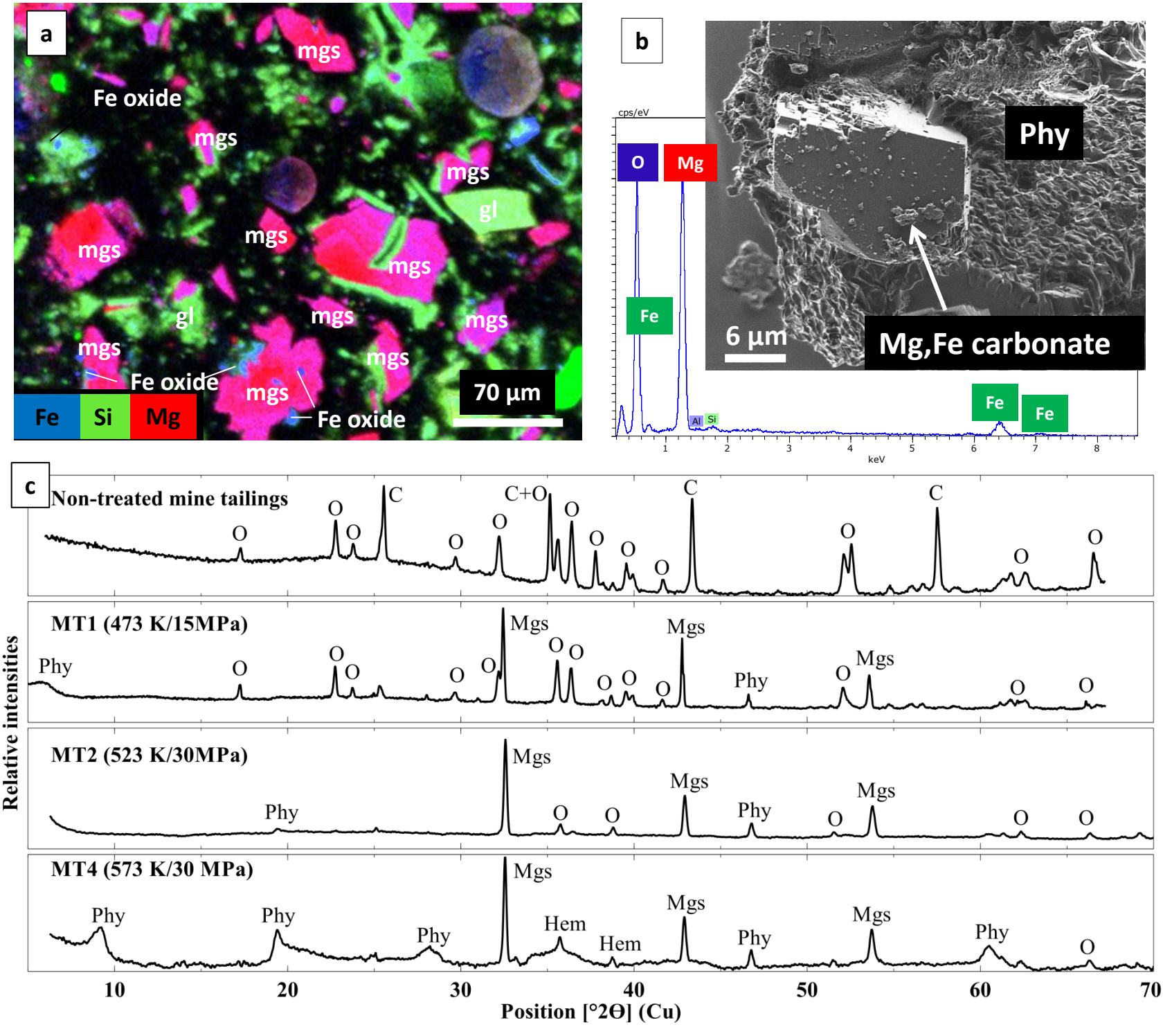
a
mgs
Fe oxide
mgs
mgs
gl
mgs
mgs
mgs
gl
mgs
mgs
mgs
mgs
Fe oxide
mgs
Fe oxide
Fe
Si
Mg
70 µm
b
cps/eV
O
Mg
Fe
Al
Si
Fe
Fe
keV
Phy
6 µm
Mg,Fe carbonate
c
Non-treated mine tailings
MT1 (473 K/15MPa)
MT2 (523 K/30MPa)
MT4 (573 K/30 MPa)
Phy
Mgs
Hem
O
C
C+O
Relative intensities
10
20
30
40
50
60
70
Position [°2Θ] (Cu)

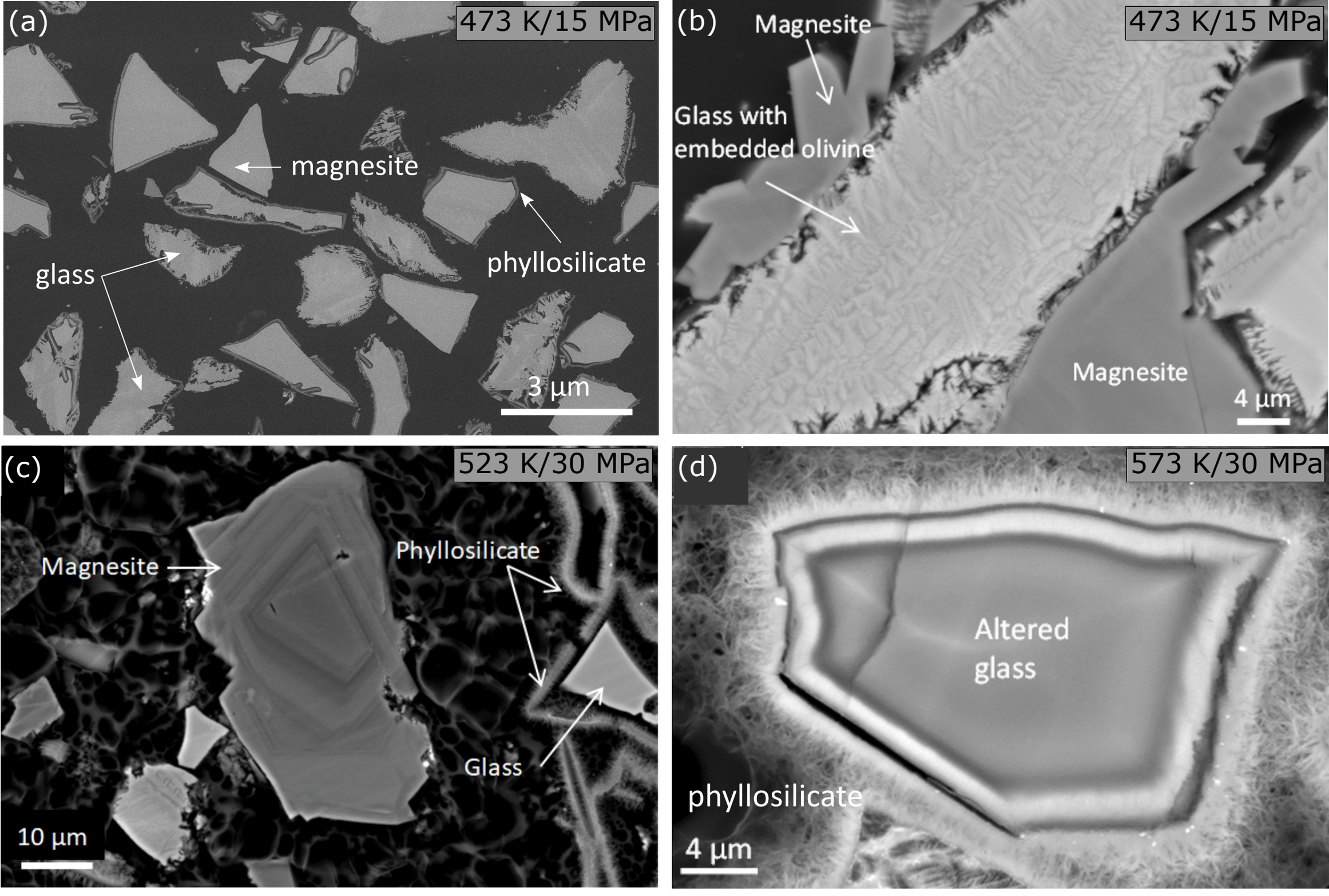
(a)
473 K/15 MPa
magnesite
phyllosilicate
glass
3 µm
(b)
Magnesite
473 K/15 MPa
Glass with
embedded olivine
Magnesite
4 µm
(c)
523 K/30 MPa
Magnesite
Phyllosilicate
Glass
10 µm
(d)
573 K/30 MPa
Altered
glass
phyllosilicate
4 µm

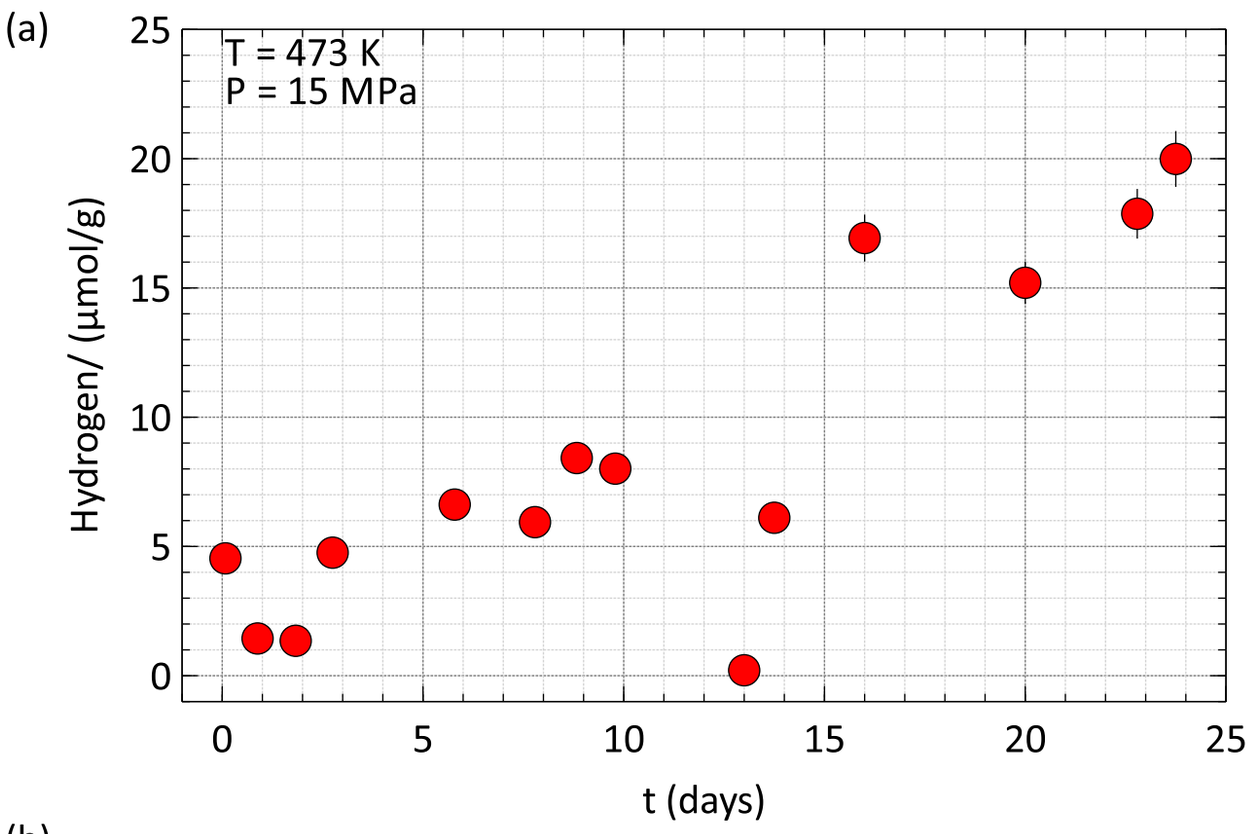
(a)
T = 473 K
P = 15 MPa
Hydrogen/ (µmol/g)
t (days)
0
5
10
15
20
25

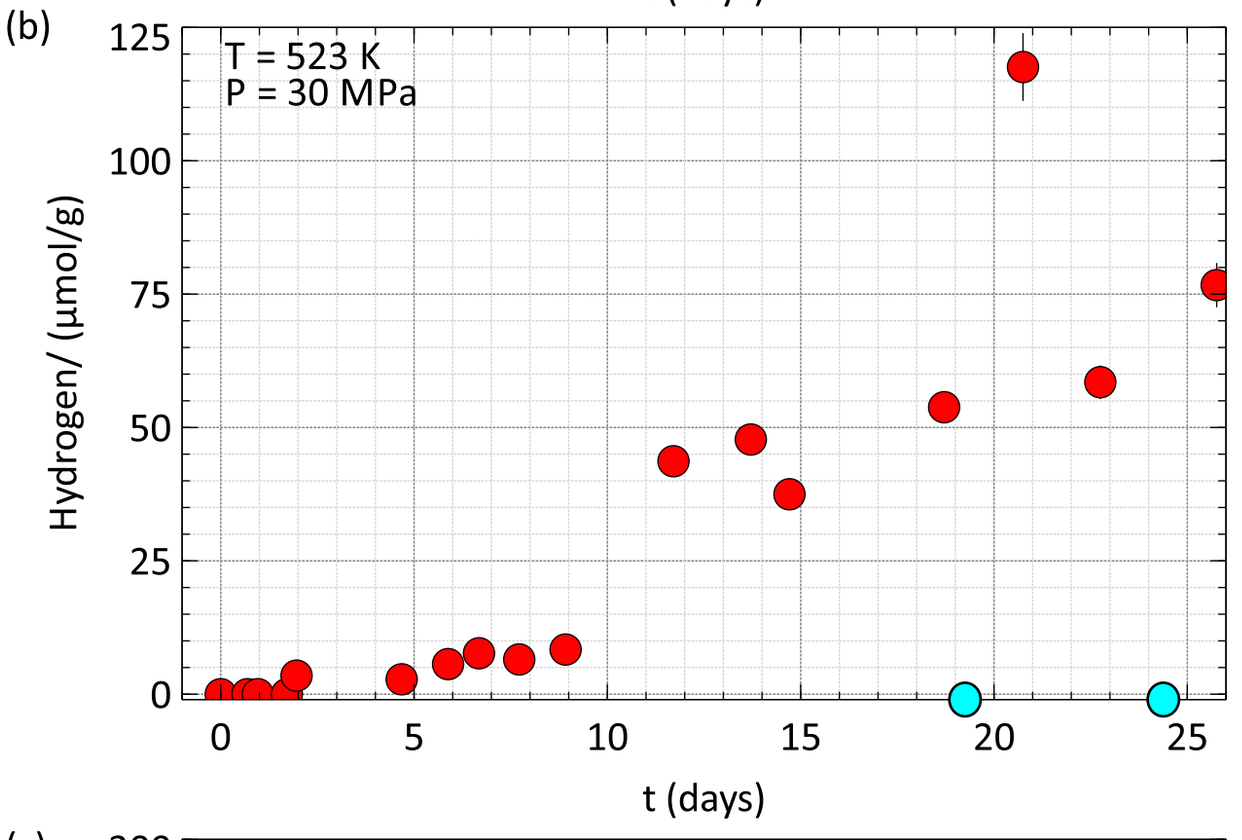
(b)
T = 523 K
P = 30 MPa
Hydrogen/ (µmol/g)
t (days)
0
25
50
75
100
125

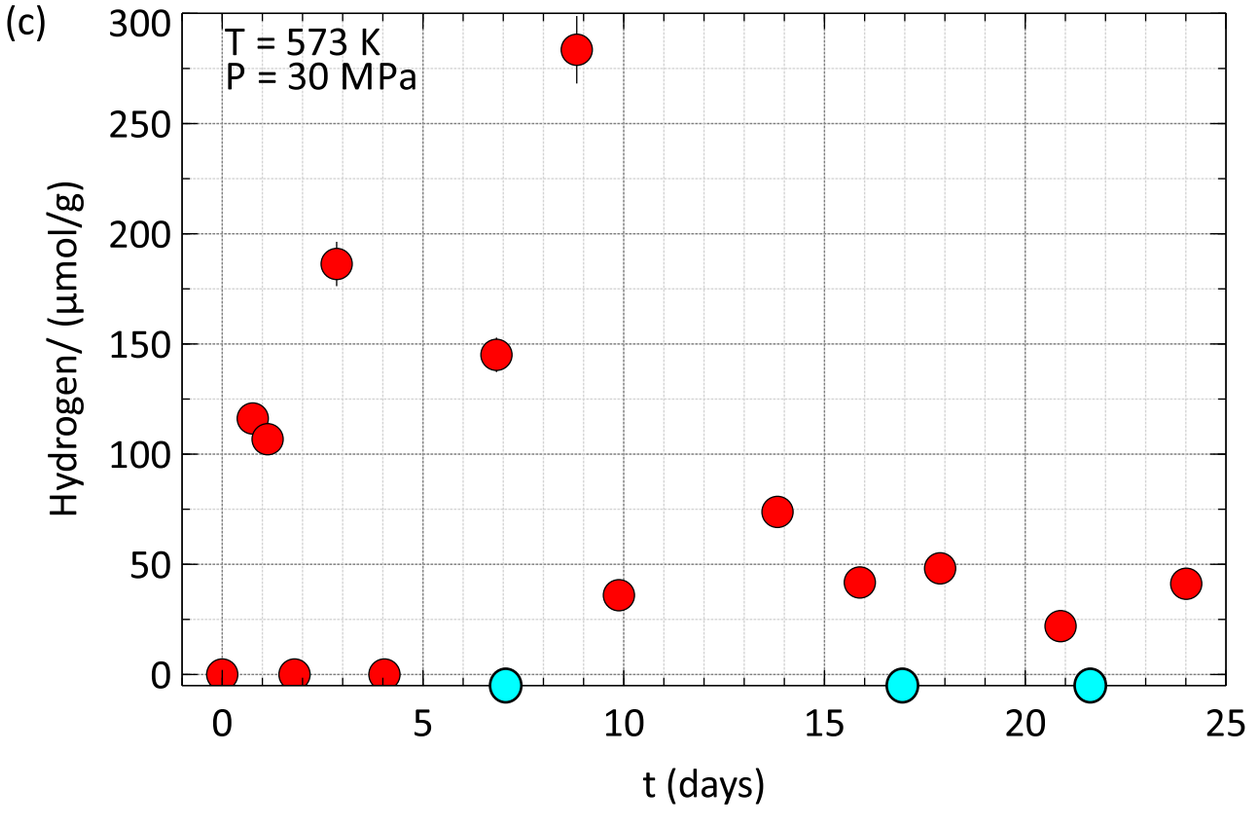
(c)
T = 573 K
P = 30 MPa
Hydrogen/ (µmol/g)
t (days)
0
50
100
150
200
250
300

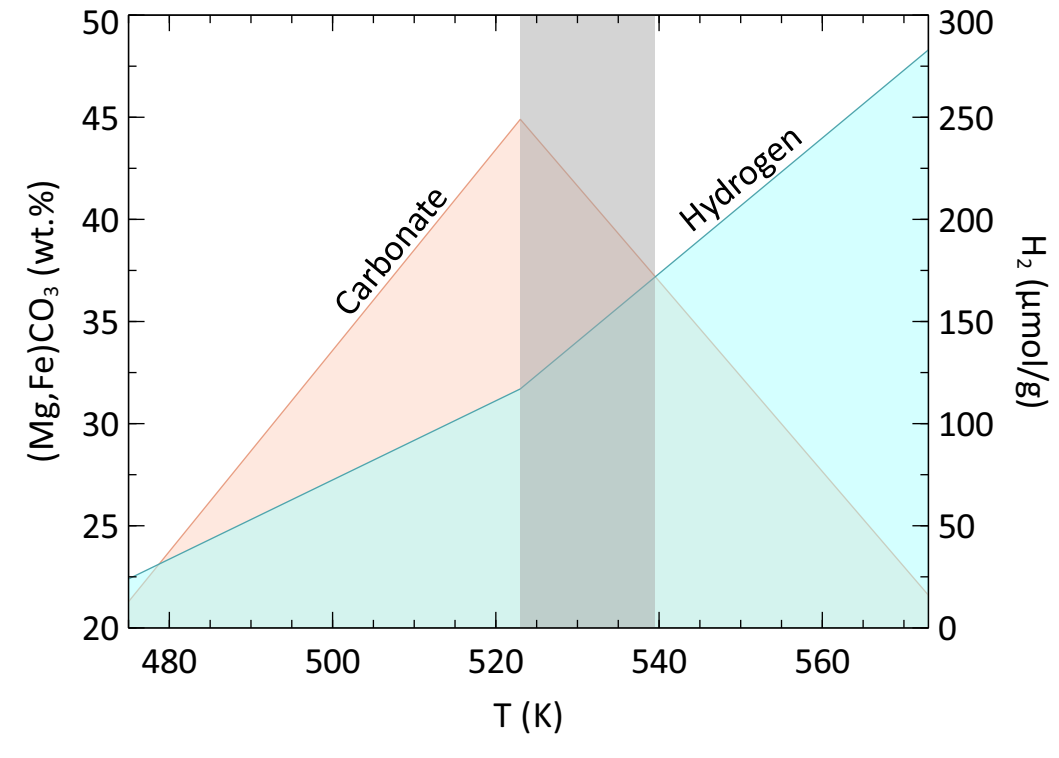
50
45
40
35
30
25
20
(Mg,Fe)CO3 (wt.%)
300
250
200
150
100
50
0
H2 (μmol/g)
Carbonate
Hydrogen
480
500
520
540
560
T (K)

Table 1. The chemical composition of New Caledonian mine tailings, determined by electron probe micro analysis (EPMA) performed on crystalline olivine and glass, expressed in weight percent (wt.%) of corresponding oxide.

	Na_2O	MgO	SiO_2	Al_2O_3	K_2O	CaO	TiO_2	Cr_2O_3	FeO	MnO	CoO	NiO	Total	Mg#[a]
Olivine	0.05	47.27	40.88	0.07	0.01	0.11	0.04	0.02	11.67	0.12	0.05	0.38	100.68	0.88
Glass	0.04	23.94	55.22	3.81	0.01	0.48	0.06	1.68	14.23	0.9	0.01	0.01	100.39	0.75
Avg[b]	0.05	35.61	48.05	1.94	0.01	0.30	0.05	0.85	12.95	0.51	0.03	0.20	100.54	0.82

[a]The magnesium number; Mg#= Mg/(Mg+Fe)

[b]Average composition of mine tailings

Table 2. Summary of experimental conditions, pH of the solutions, carbonate yields, measured hydrogen and methane in each batch experiment.

	P(total) (MPa)	$P(CO_2)$[a] (MPa)	T (K)	t (days)	Mine tailings (g)	Pure water (g)	water/rock ratio	Initial pH[c]	CO_2 storage[d] (g/kg)	Hydrogen(max) measured by GC (g/kg)[e]	Methane(max) (g/kg)[e]
MT1	15	13.1	473	25	2.0	201	100	3.55	114.4	0.04	nd
MT2	30	26.4	523	25	1.7	170	100	3.65	320.5	0.24	0.02
MT4	30	28.2	573	24	1.7	170	100	3.94	118.5	0.57	0.05
MT2b (blank)	30	26.4	523	24	-	170	-	-	nd	nd	0.01
MT4b (blank)	30	28.2	573	24	-	170	-	-	nd	nd	0.06

[a]Calculated for the given temperature and P(total) using the thermosolver software (Barnes and Koretsky, 2004)
[b]Solid mass to solution volume ratio
[c]pH at experimental conditions calculated using the CHESS geochemical code (van der Lee and De Windt, 2002)
[d]grams of molecular CO_2 trapped in 1 kg of mine tailings
[e]grams of hydrogen (H_2), or methane (CH_4) produced per 1kg of mine tailings
nd = not detected in the gas chromatography analysis

Table 3. Production of hydrogen in each experiment estimated from FeO analysis. Reaction progress calculated based on the hydrogen production is also reported (Rx%).

Exp.	Wt (g)	T (K)	FeO wt%	FeO (mmol/g)	ΔFeO (mmol/g)*	Eq. H_2[a] (µmol/g)	Eq. H_2 (g/kg)	Rx%
MT[b]	2	-	9.39	1.31	0	no		
MT1	2	473	9.65[c]	1.34	-0.03	-15	-0.03	-2.3
MT2	2	523	7.74	1.08	0.23	115	0.23	17.6
MT4	2	573	5.61	0.78	0.53	265	0.53	40.5

[a]Equivalent hydrogen

[b]MT refers to non-treated mine tailings

[c]This is an analytical error (see text), causing the successive negative values.

Table 4. Comparison of ex-situ CO_2 sequestration at 573K <T>423 K and P<30 MPa

Composition	d (μm)	P (MPa)	T (K)	t (h)	Solution	CO_2 (g/kg)[a]	Reference
chrysotile (OK)	425-1000	12.4	428	1	1M NaCl, 0.64M $NaHCO_3$	183.0	Bobicki et al., 2015
chrysotile (Pipe)	425-1000	12.4	428	1	1M NaCl, 0.64M $NaHCO_3$	157.0	Bobicki et al., 2015
Olivine	20-80	15	423	336	supercritical CO_2	261.0	Garcia et al.,2010
Olivine	40-63	15	473	600	CO_2-saturated water	114.4	This study_MT1
Olivine	40-63	30	523	600	CO_2-saturated water	320.5	This study_MT2
Olivine	40-63	30	573	576	CO_2-saturated water	118.5	This study_MT4

[a]Grams of molecular CO_2 captured by one kg of starting material

Table 5. Comparison of hydrogen production by experiments conducted at 473 and 573 K.

Reference	Material	Solution	pH	T	t (h)	[b](H_2 g/kg)
Malvoisin et al., 2013	[a]CARBOF	water	6.9	473	69.2	0.01
Crouzet et al., 2017	FeO	0.05M acetic	3	473	72	5.34
This study	mine tailings	CO_2+water	3.6	473	66	0.07
Malvoisin et al., 2013	CARBOF	water	6.9	573	141	1.38
Crouzet et al., 2017	FeO	water	6	573	144	2.18
This study	mine tailings	CO_2+water	3.9	573	164	2.26

[a]CARBOF=carbonated basic oxygen furnace steel slag

[b]grams of H_2 produced by 1 kg of FeO

Highlights

- New Caledonian mine tailings can be used for ex-situ CO_2 sequestration and H_2 production.
- Mg and Fe incorporation among the secondary phases play an important role.
- Maximum yields obtained at 523 K and 540 K at pCO_2=30 MPa.
- A novel method of valorization of Fe, Mg containing mine tailings.
- Cost effective method to treat CO_2 emissions and energy demands.